

AD-A194 758

NSWC TR 86-498



N 5/13
KTI GRW SPY
T2 EPM
T4 CEC
FILE #

A

COMPUTER MODELING OF A BOOSTER IN AN ARTILLERY SHELL

BY J. O. ERKMAN M. LUTZKY

RESEARCH AND TECHNOLOGY DEPARTMENT

1 DECEMBER 1986

Approved for public release; distribution is unlimited.



NAVAL SURFACE WEAPONS CENTER

Dahlgren, Virginia 22448-5000 • Silver Spring, Maryland 20903-5000

UNCLASSIFIED

SECURITY CLASSIFICATION OF THIS PAGE

REPORT DOCUMENTATION PAGE

1a. REPORT SECURITY CLASSIFICATION Unclassified		1b. RESTRICTIVE MARKINGS	
2a. SECURITY CLASSIFICATION AUTHORITY		3. DISTRIBUTION/AVAILABILITY OF REPORT Approved for public release; distribution unlimited.	
2b. DECLASSIFICATION/DOWNGRADING SCHEDULE			
4. PERFORMING ORGANIZATION REPORT NUMBER(S) NSWC TR 86-498		5. MONITORING ORGANIZATION REPORT NUMBER(S)	
6a. NAME OF PERFORMING ORGANIZATION Naval Surface Weapons Center	6b. OFFICE SYMBOL <i>(If applicable)</i> R12	7a. NAME OF MONITORING ORGANIZATION	
6c. ADDRESS (City, State, and ZIP Code) 10901 New Hampshire Avenue Silver Spring, MD 20903-5000		7b. ADDRESS (City, State, and ZIP Code)	
8a. NAME OF FUNDING / SPONSORING ORGANIZATION	8b. OFFICE SYMBOL <i>(If applicable)</i>	9. PROCUREMENT INSTRUMENT IDENTIFICATION NUMBER	
8c. ADDRESS (City, State, and ZIP Code)		10. SOURCE OF FUNDING NUMBERS	
		PROGRAM ELEMENT NO. 63610N	PROJECT NO. S0199-AS
		TASK NO.	WORK UNIT ACCESSION NO. 2U22CA
11. TITLE <i>(Include Security Classification)</i> Computer Modeling of a Booster in an Artillery Shell			
12. PERSONAL AUTHOR(S) Erkman, J. O., and Lutzky, M.			
13a. TYPE OF REPORT	13b. TIME COVERED FROM _____ TO _____	14. DATE OF REPORT (Year, Month, Day) 1986 December 1	15. PAGE COUNT 62
16. SUPPLEMENTARY NOTATION			
17. COSATI CODES	18. SUBJECT TERMS <i>(Continue on reverse if necessary and identify by block number)</i> Booster Transfer, Artillery Shells, Detonation, Explosive, Reliability, M732 Fuze, WONDY IV, Shock, Spall		
FIELD 19 20	GROUP 04	SUB-GROUP 11	
19. ABSTRACT <i>(Continue on reverse if necessary and identify by block number)</i>			
<p>Results are given for computer simulation of the Army's M732 Artillery Proximity Fuze. The simulations were done in a study of the reliability of the detonation of the explosive in the artillery shell by the fuze. Because the computer code used--WONDY IV--integrates the differential equations of flow in one-dimension, a simplified model of the fuze was used. The quantity of $p^2\tau$ was evaluated for each of the several models for comparison with experimental results found in the literature for TNT. When this quantity, which is the integral of $p^2 d\tau$, exceeds a value $p^2\tau_{critical}$, the explosive is expected to detonate reliably.</p> <p>In the appendix, the example, which includes a plate of steel (stainless here), is examined extensively to show how stress waves propagate and interact in a multilayered configuration. These results should be of interest to both computer simulators of explosive events and to designers of booster hardware.</p>			
20. DISTRIBUTION/AVAILABILITY OF ABSTRACT <input checked="" type="checkbox"/> UNCLASSIFIED/UNLIMITED <input type="checkbox"/> SAME AS RPT. <input type="checkbox"/> DTIC USERS		21. ABSTRACT SECURITY CLASSIFICATION Unclassified	
22a. NAME OF RESPONSIBLE INDIVIDUAL John O. Erkman		22b. TELEPHONE <i>(Include Area Code)</i> (202) 394-1177	22c. OFFICE SYMBOL R12

UNCLASSIFIED

SECURITY CLASSIFICATION OF THIS PAGE

UNCLASSIFIED

CLASSIFICATION OF THIS PAGE

FOREWORD

The work reported here was done at the request of the Army Research and Development Command. The purpose of the work was to evaluate the reliability of the Army's M732 Artillery Proximity Fuze in a new application. The evaluation was done both by experimentation and by computer modeling. Results concerning reliability are reported in NSWC TR 82-62, Reference 1 of this report. Because of the wide applicability of computer modeling in fuze and warhead design, this report gives details of the modeling effort. The method used was general enough to serve as a guide for those who will use computer modeling in the future. It demonstrates how complicated wave interaction becomes in a rather simple system. It also shows how a criterion for detonation can be obtained from a computer simulation. In this case we used the familiar $p^2\tau$ criteria.

Approved by:

K. F. Mueller
K. F. MUELLER, Head
Energetic Materials Division

BLANK

CONTENTS

	<u>Page</u>
INTRODUCTION	1
THE COMPUTER PROGRAM	6
THE EQUATIONS OF STATE	7
DETONATING THE EXPLOSIVE	8
DISCUSSION OF RESULTS	9
DISCUSSION	21
REFERENCES	22
APPENDIX A--COMMENTS ON THE INTERACTION OF WAVES IN A SPHERICAL MODEL OF A BOOSTER	A-1
DISTRIBUTION	(1)

ILLUSTRATIONS

<u>Figure</u>		<u>Page</u>
1	M732 FUZE CONFIGURATION	2
2	FUZE COMPONENTS, M732	3
3	SIMPLIFIED CONFIGURATION OF THE BOOSTER	4
4	COMPUTATIONAL MODEL USED IN THE CODE FOR FLOW IN ONE-DIMENSION	5
5	CASE 1, NO AIR GAP.	12
6	CASE 2, AIR GAP = 0.051 CM.	13
7	CASE 3, AIR GAP = 0.229 CM.	14
8	CASE 4, HEAD HEIGHT = 1.12 CM	15
9	CASE 5, HEAD HEIGHT = 1.27 CM	16
10	CASE 6, ALUMINUM BOOSTER CUP THICKNESS = 0.2032 CM.	17
11	CASE 7, STAINLESS STEEL BOOSTER CUP	18
12	CASE 8, ZINC BOOSTER CUP.	19
A-1	COMPUTATIONAL MODEL USED IN THE CODE FOR FLOW IN ONE-DIMENSION. .	A-9
A-2	DISTANCE VS TIME FOR WAVE INTERACTION IN COMPUTER MODEL OF BOOSTER	A-10
A-3	PRESSURE AND DISTANCE VS TIME FOR PARTICLE PATH L1.	A-11
A-4	PRESSURE AND DISTANCE VS TIME FOR PARTICLE PATH L2.	A-12
A-5	PARTICLE VELOCITY AND DISTANCE VS TIME FOR PARTICLE PATH L1 . .	A-13
A-6	PARTICLE VELOCITY AND DISTANCE VS TIME FOR PARTICLE PATH L2 . .	A-14
A-7	DISTANCE VS TIME FOR WAVE INTERACTIONS IN THE COMPUTER MODEL SHOWING EFFECT OF SPALLING.	A-15

ILLUSTRATIONS (Cont.)

<u>Figure</u>		<u>Page</u>
A-8	PRESSURE AND DISTANCE VS TIME FOR PARTICLE PATH L3.	A-16
A-9	PRESSURE AND DISTANCE VS TIME FOR PARTICLE PATH L4.	A-17
A-10	PRESSURE AND DISTANCE VS TIME FOR PARTICLE PATH L5.	A-18
A-11	PRESSURE AND DISTANCE VS TIME FOR PARTICLE PATH L6.	A-19
A-12	PRESSURE AND DISTANCE VS TIME FOR PARTICLE PATH L7.	A-20
A-13	PRESSURE AND DISTANCE VS TIME FOR PARTICLE PATH L8.	A-21
A-14	PARTICLE VELOCITY AND DISTANCE VS TIME FOR PARTICLE PATH L3 . . .	A-22
A-15	PARTICLE VELOCITY AND DISTANCE VS TIME FOR PARTICLE PATH L4 . . .	A-23
A-16	PARTICLE VELOCITY AND DISTANCE VS TIME FOR PARTICLE PATH L5 . . .	A-24
A-17	PARTICLE VELOCITY AND DISTANCE VS TIME FOR PARTICLE PATH L6 . . .	A-25
A-18	PARTICLE VELOCITY AND DISTANCE VS TIME FOR PARTICLE PATH L7 . . .	A-26
A-19	PARTICLE VELOCITY AND DISTANCE VS TIME FOR PARTICLE PATH L8 . . .	A-27

TABLES

<u>Table</u>		<u>Page</u>
1	EQUATION OF STATE DATA	8
2	JWL EQUATION OF STATE PARAMETERS FOR PBX-9407	8
3	CRITICAL ENERGY FOR DETONATION FOR TNT.	10
4	ALUMINUM FLYER PLATE AGAINST COARSE GRAIN TNT	10
5	DIMENSIONS OF MODELS AND RESULTS.	11
A-1	LOCATIONS OF FRACTURES, CLOSURES AND SPALL TENSIONS	A-6

INTRODUCTION

The Army's M732 Artillery Proximity Fuze (see Figures 1 and 2) reliably initiates standard 5"/54 projectiles filled with explosives A-3, Comp B, and pressed TNT. The Army Research and Development Command (ARADCOM) requested that the reliability of initiating 5"/54 projectiles with cast TNT be evaluated in conjunction with a plan to use the M732 fuze with cast TNT British projectiles. The Naval Surface Weapons Center (NSWC) conducted an experimental and computational program to evaluate reliability (reported in NSWC TR 82-20).¹ To achieve reliable initiation of cast TNT, it is necessary to modify the fuze design. The results of the experimental program are presented in NSWC TR 82-20. This report documents the computational model. Generally, the mechanical linkages of a fuze are too complex to be modeled on a computer. However, the design may be approximated by a simple model as will be shown later. Computations can be used to investigate fuze designs (dimensions, tolerances, and materials). The results of the hydrodynamic modeling are presented here.

The M732 fuze depicted in Figures 1 and 2 was idealized to the configuration of Figure 3. All of the components from the S and A module (see Figure 1) to the oscillator assembly were presumed to function properly and, therefore, omitted from the idealized configuration. The idealized configuration consisted of a thin disc of booster explosive (CH-6) inserted in a booster cup assembly (cylindrical metal dish). The depth of the booster cup assembly equaled the thickness of the CH-6 disc; the inner diameter of the booster cup assembly equaled the diameter of the explosive disc. The idealized configuration assumes point initiation of the CH-6 on its centerline, where the actual M732 booster explosive is initiated by a lead cup assembly approximately 0.20 inches in diameter.

Since the booster pellet (disc) is very thin, a point initiated detonation wave will reach the bottom of the booster cup assembly (and the acceptor explosive) before reaching the side wall of the booster cup assembly. Hence, the acceptor explosive is shocked by a spherically expanding wave. Because of this, it was thought to be sufficient to use a code for flow in one dimension. Therefore, the model used for the computer simulation is as depicted in Figure 4. Region 1 represents the CH-6 booster charge. Region 2 represents the booster cup now given some radius of curvature due to the spherically symmetric approximation being made. Region 3 corresponds to an air gap left when the fuze is inserted into a projectile. Region 4 is the barrier disc, also given an artificial radius of curvature. Region 5 is the acceptor explosive which the fuze is intended to detonate.

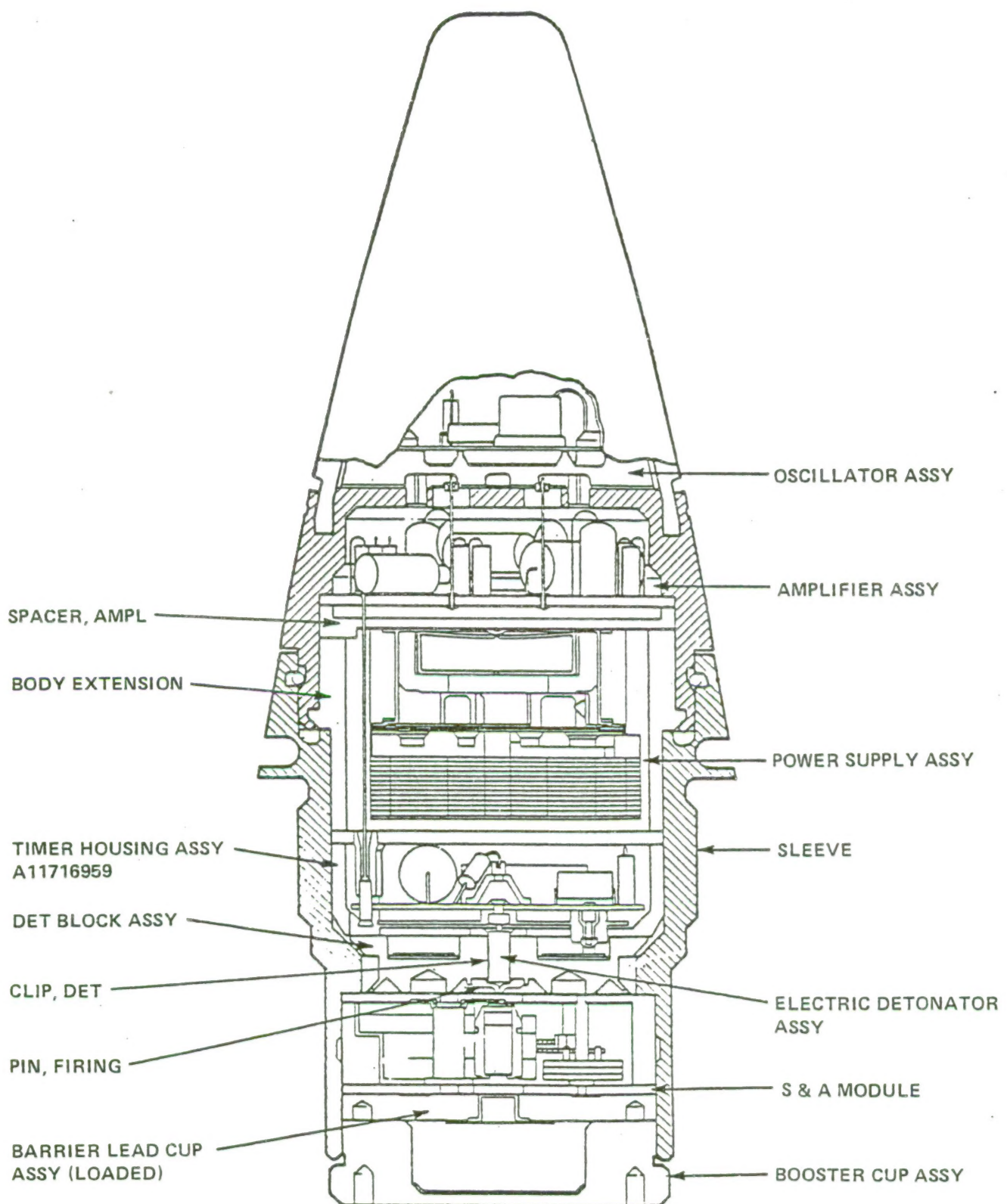


FIGURE 1. M 732 FUZE CONFIGURATION

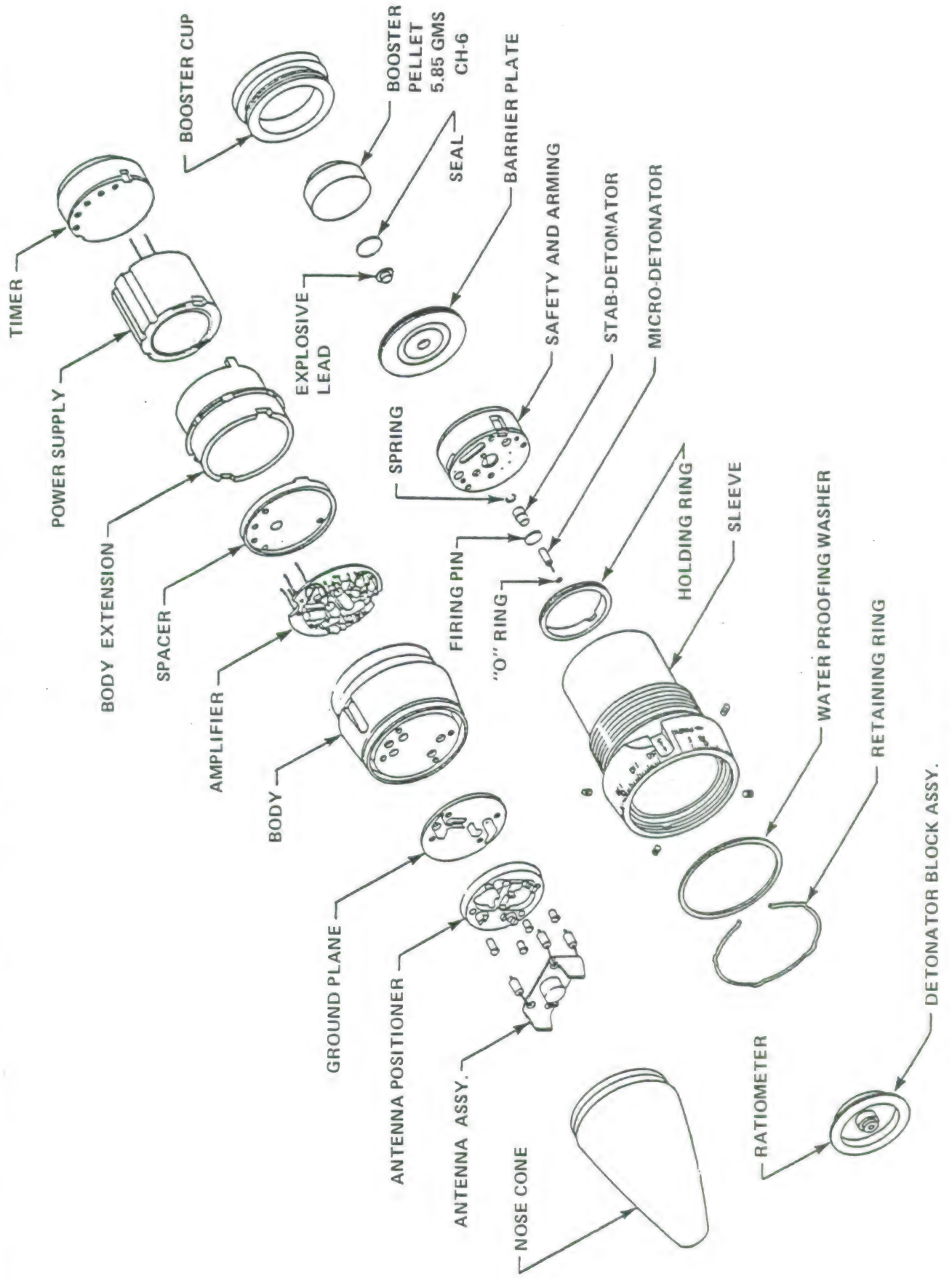


FIGURE 2. FUZE COMPONENTS, M 732

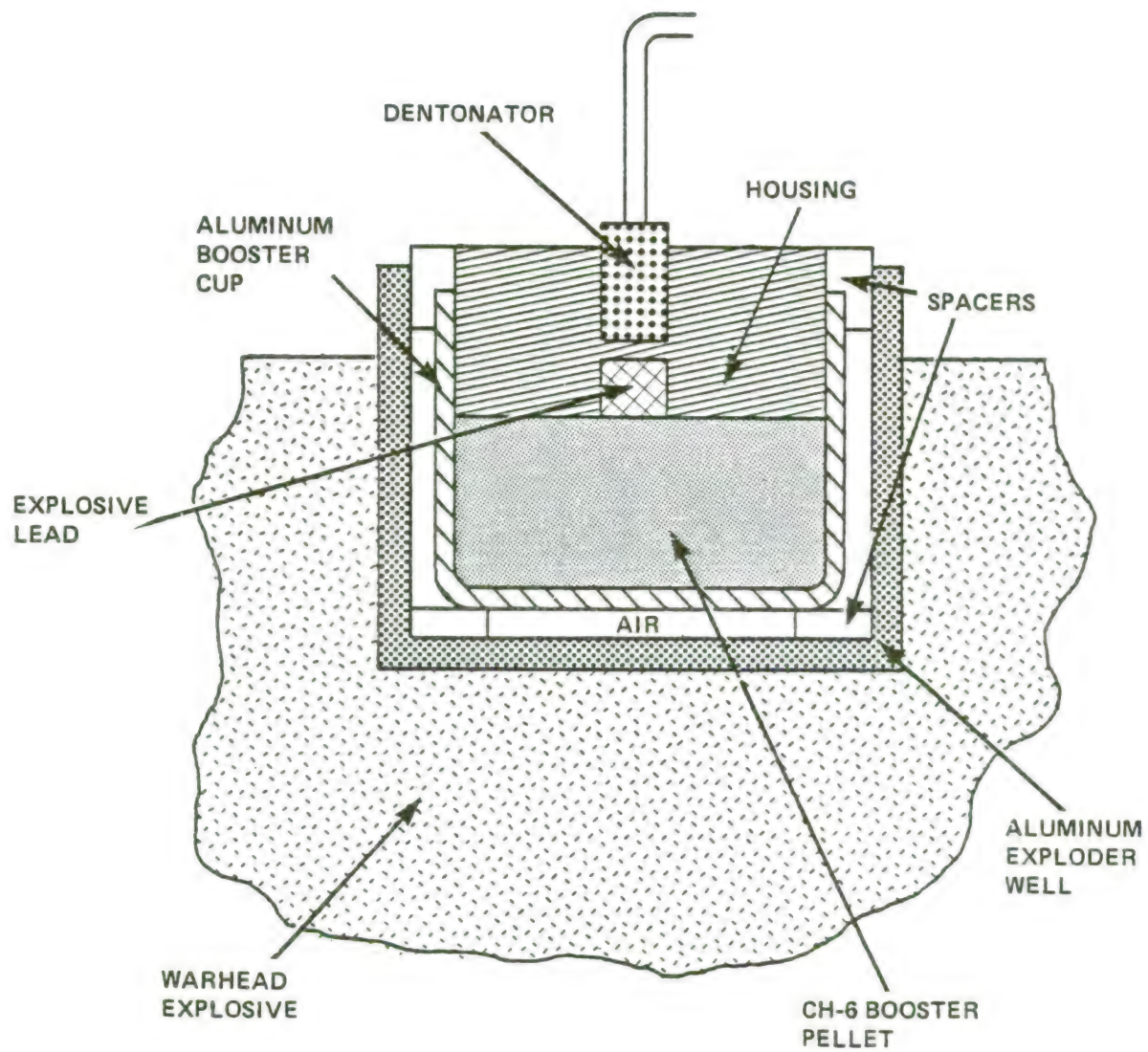
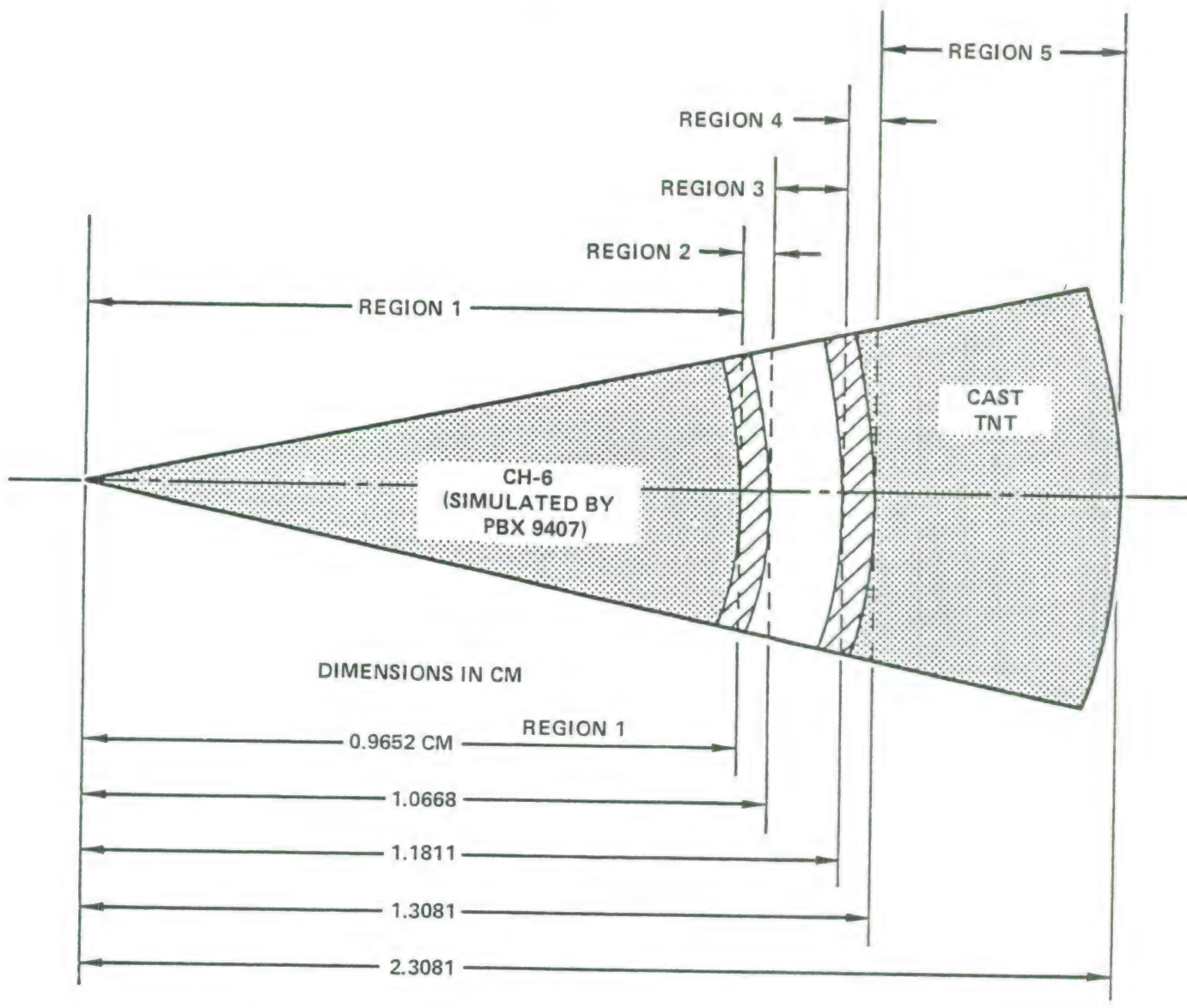


FIGURE 3. SIMPLIFIED CONFIGURATION OF THE BOOSTER



REGION	ZONE ALLOCATION	MATERIAL	REGION THICKNESS		ZONE THICKNESS CM
			CM	INCHES	
1	1 THROUGH 124	PBX 9407	0.9652	0.380	0.0078
2	125 THROUGH 151	ALUMINUM	0.1016	0.040	0.0040
3	VOID	AIR GAP	0.143	0.045	-
4	152 THROUGH 183	ALUMINUM	0.127	0.050	0.0042
5	184 THROUGH 283	TNT (NON-REACTIVE)	1.0	0.394	0.0100

FIGURE 4. COMPUTATIONAL MODEL USED IN THE CODE FOR FLOW IN ONE-DIMENSION

Figure 4 gives relevant dimensions, and zone and region assignments for a typical computation. It should be noted that regions 1, 2, 4, and 5 are divided into zones. Region 3 is designated as "void," and because region 3 is massless compared to the metal structures and the explosives, it needs no zoning. The "detonation" commences at zone 1 and sweeps through region 1 (the booster). The detonation wave of region 1 drives a non-reactive shock in the aluminum booster cup (region 2), causing it to move across the void (region 3). Eventually the moving aluminum body strikes the aluminum exploder well (region 4), forming a shock wave which travels through that region and finally into the not-yet-reacting warhead explosive (region 5).

The hydrodynamic data for the booster explosive (region 1) were approximated conservatively. The tactical explosive is CH-6 at a density of 1.614 to 1.628 g/cm³, CH-6 being an RDX explosive with 2.5 percent of diluent. We used the Jones, Wilkins, and Lee (JWL) equation of state for PBX-9407 at a density of 1.60 g/cm³; PBX-9407 is also an RDX explosive, but with 6 percent diluent. Since we used data for a weaker (more dilute and less dense) explosive, the computed shock levels can err only on the low side. This is a very conservative prediction of detonation-transfer reliability.

The transfer of a detonation wave from the booster explosive to the acceptor explosive was modeled using the computer code WONDY IV² which computes flow in one dimension.

Among the design variations modeled was the booster cup metal. Aluminum, zinc and steel were considered. Stainless steel was used instead of mild steel because of the difficulty of developing an equation of state for mild steel due to the presence of a phase transition. Other design variations include thickness of explosives, metals, and air gaps.

The quantities calculated with WONDY IV include space-time histories of each interface, pressure time history of the interfaces, and velocity of the interfaces. With this information, the $p^2\tau$ shock initiation criteria was used to assess reliability.

THE COMPUTER PROGRAM

The computer program used for the calculations is known as WONDY IV.² The program integrates the differential equations which describe the propagation of waves of finite amplitude. It belongs to the class of codes sometimes referred to as artificial viscosity codes or Q-codes or hydrocodes. These codes introduce an artificial viscosity so that a discontinuity that would otherwise be a shock front, is spread out in space over a few zones or cells. This procedure greatly simplifies the computational process because shocks (and other discontinuities) are treated with the same equations as are continuous waves, e.g., a rarefaction wave. The loss of accuracy, for example, at a shock front, is more than compensated for by the simplicity of such codes.

THE EQUATIONS OF STATE

The WONDY IV code makes use of what is usually called a Mie-Gruneisen type equation of state. Equations of state (EOS) are provided for solids, explosives, and perfect gases. The EOS for solids used in these calculations can describe elastic-plastic flow. This EOS uses the Hugoniot of a material for input that is usually done by describing the Hugoniot as a linear relation between the shock and particle velocities. Other input data required by the code are the bulk modulus, K , the shear modulus, G , the yield strength, Y_0 , and the Gruneisen ratio, Γ . Any of these four may be expressed as variables dependent on the state in the solid. In the computations described in this report, Γ was allowed to vary with specific volume, V , in the following way:

$$\Gamma V = \Gamma_0 V_0 \quad (1)$$

where the subscript means the value of the parameter at ambient conditions. The parameters C_0 , the initial bulk sound speed, and s relate the shock velocity U , and the particle velocity u by

$$U = C_0 + su \quad . \quad (2)$$

Values of the equation of state parameters are given in Table 1. Here TNT is represented as a non-detonating material.

The yield strength Y_0 , is the stress at which the material is no longer elastic. The adiabatic bulk modulus at zero pressure and room temperature is calculated from

$$K_0 = \rho_0 C_0^2 \quad (3)$$

where the subscript 0 refers to the ambient state and ρ_0 is the ambient density. Similarly

$$G_0 = 3K_0(1-2\nu)/(2(1-\nu)) \quad (4)$$

where ν is the Poisson ratio, here taken to be 0.333 for stainless steel and aluminum, and 0.0 for non-detonating TNT. Values of the parameters ρ_0 , Γ_0 , C_0 and s are given in Table 1 for stainless steel (SS), aluminum and unreacted TNT.

TABLE 1. EQUATION OF STATE DATA

Material	Density g/cm ³	C ₀ cm/ μ sec	s	Γ	v	Y ₀ megabar
STAINLESS STEEL ³	7.896	0.4569	1.49	2.17	0.33	0.006
TNT ⁴	1.614	0.239	2.05	0.737	0.0	0.0
Al(6061) ⁵	2.70	0.537	1.34	2.10	0.33	0.003
ZINC ⁶	7.14	0.365	1.559	2.45	0.33	0.0

For some explosives, the behavior of the detonation product gases is described by the JWL equation of state.⁷ This is an empirically derived relation involving the pressure, p, the density, ρ , and the energy E. The relation is as follows:

$$p = A \left(1 - \frac{\omega_0}{R_1 \rho_0}\right) e^{-R_1 \rho_0 / \rho} + B \left(1 - \frac{\omega_0}{R_2 \rho_0}\right) e^{-R_2 \rho_0 / \rho} + \frac{\omega_0^2}{\rho_0} E, \quad (5)$$

where A, B, ω , R₁, and R₂ are fixed parameters for any particular explosive. Table 2 gives the values for the equation of state parameters for PBX-9407. The explosive energy is put into the array for each cell during the initialization of the computations.

TABLE 2. JWL EQUATION OF STATE PARAMETERS FOR PBX-9407⁸

EXPLOSIVE	ρ_0 (g/cm ³)	D (cm/ μ s)	A (mbar)	B (mbar)	R1	R2	W	E_0 (mbar-cm ³ /cm ³)
PBX-9407	1.6	0.791	5.73187	0.14639	4.6	1.4	0.32	0.0538

DETONATING THE EXPLOSIVE

The energy of the explosive can be released in three different ways by the code. One way is described as the "time to burn" scheme.⁷ At the start of the computations, the distance from the point of detonation (center of the sphere of explosive in the work given here) to each cell is calculated. The

time that a particular cell releases energy is then determined by dividing the distance by the detonation velocity. A viscosity type parameter spreads the "detonation" front over three or four cells so that the equations for continuous flow can be used.

The scheme described above is used when the time and position are known for initiation. This is not known in cases in which a plate or projectile impacts an explosive, or when a detonation passes from one explosive to another. For such an event, a volume fraction is used as the criterion for release of the energy of a cell of explosive.⁷ As the explosive is compressed by impact of a projectile, or by the detonation of an adjacent explosive, the parameter

$$F = (1 - V/V_0) \div (1 - V_{CJ}/V_0) \quad (6)$$

is computed. Here V is the specific volume of the compressed material, V_{CJ} is the specific volume of the explosive at the Chapman-Jouguet (CJ) plane, and V_0 is the specific volume of the undetonated explosive. Initially F is zero. When its value becomes 0.05, a fraction of the energy in the cell is released. More energy is released as the pressure is increased during successive steps in time. After a time the value of F for a given cell becomes equal to, or greater than 1.0. When this happens, F is set to 1.0, and no further energy is released from that cell. A viscosity-like parameter is used to spread the detonation front over several cells, so that the equations for continuous flow can be used.

DISCUSSION OF RESULTS

In order to predict whether a particular pressure wave will initiate an explosive, a criterion relating the transient conditions in the wave to the detonation formation must be available. It was first noticed by Hubbard and Johnson,⁹ using numerical calculations, that for square pressure pulses of given height, there exists a minimum pulse duration required to obtain detonation. Subsequently, Walker and Wasley¹⁰ proposed an initial energy criterion for detonation. This implied that initiations would be achieved if the wave was such that a certain critical value of the quantity $p^2\tau$ was exceeded. Here p is the pressure of the square pulse, and τ is the pulse duration. This criterion is referred to as the $p^2\tau$ criterion. Although originally conceived for a square pulse, the criterion is sometimes applied when the pulse is not square. In this case, it is assumed that the critical quantity is given by the integral of p^2 with respect to time. This is the way the criterion will apply in this report. It should be noted that the sensitivity of explosives is not well understood, and that many different phenomena can enter into the determination of when an explosive will detonate. However, various experimental studies of the $p^2\tau$ criterion suggest that it is at least a plausible criterion to use, and will produce dependable order of magnitude correlations between pressure waves with $p^2\tau$ larger than the critical value and the initiation of detonation.

In order to use the $p^2\tau$ criterion to evaluate the computations previously described, there must be available a value of $p^2\tau$ (critical) for TNT from experimental observations. Such data are scarce, and only one source

will be used here. Taylor and Erwin¹¹ gave results from plate impact experiments; these results are given in Tables 3 and 4. The tables are self explanatory. Recall that the equation of state used for TNT in the calculations was for cast TNT which had a density of 1.614 g/cm³. The greatest density for TNT in the two tables is 1.55 g/cm³ for pressed charges. Note that the values of $p^2\tau$, called $p^2(\Delta\tau)$ by Taylor, depend on the density of the TNT, on the coarseness of the TNT before pressing, and the thickness of the flyer plate. The value 324.0 kbar²-μsec is given in the first column of Table 3.

TABLE 3. CRITICAL ENERGY FOR DETONATION FOR TNT

Flyer Plate Thickness (in. nominal)	0.040	0.040	0.040	0.125
Flyer Plate Kinetic Energy (cal/cm ²)	22.0	23.2	43.	60.1
Explosive Density (g/cm ³)	1.55	1.55	1.3	1.3
Grain Size	Fine	Coarse	Coarse	Coarse
Explosive Pressure (Kbar)	29.5	30.5	32.0	18.2
Explosive Particle Velocity (mm/μsec)	0.578	0.592	0.871	0.627
Pulse Time (μsec)	0.372	0.371	0.370	1.142
$P_u(\Delta t)$ (cal/cm ²)	15.2	16.0	24.6	31.1
$P^2(\Delta t)$ (kbar ² -μsec)	324.	346.	378.	378.

TABLE 4. ALUMINUM FLYER PLATE AGAINST COARSE GRAIN TNT
($\rho = 1.30$ g/cm³)

Flyer Plate Thickness (in. nominal)	0.040	0.125	0.125	0.125	0.125	0.125	0.125
Flyer Plate Kinetic Energy (cal/cm ²)	43.0	45.3	51.3	54.2	56.2	60.1	63.4
Reaction Products Velocity (mm/μsec)	9.75	6.28	7.60	8.17	8.87	9.42	9.57
Explosive Pressure (kbar)	32.0	14.7	16.1	16.8	17.4	18.2	19.0
Explosive Particle Velocity (mm/μsec)	0.871	0.553	0.584	0.598	0.611	0.627	0.643
Pulse Time (μsec)	0.370	1.149	1.145	1.145	1.142	1.142	1.138
$P_u(\Delta t)$ (cal/cm ²)	24.6	22.2	25.8	27.5	29.0	31.1	33.2
$P^2(\Delta t)$ (kbar ² -μsec)	378	247	298	323	346	378	411

The first set of computations involves a series in which the size of the air gap between the booster cup and exploder well is varied. In all cases the radius of the booster charge, PBX-9407, is 0.965 cm, the thickness of the booster cup (aluminum) is 0.102 cm, and the thickness of the exploder well (aluminum) is 0.127 cm. These are values for the baseline design. For case 1 the air gap = 0 cm. The pressure-time profile obtained at a point in the TNT acceptor adjacent to the exploder well interface is shown in Figure 5. The calculated integral of $p^2\tau$ is 2780 kbar 2 -usec, where the integral was evaluated over a time interval of 2.31 usec. The peak pressure was 100 kbar. In case 2 the air gap was 0.051 cm, and the $p^2\tau$ integral, evaluated over an interval of 2.31 usecs, is equal to 2580 kbar 2 -usec. The pressure-time profile is given in Figure 6, and we see that the peak pressure achieved was 111 kbar. Finally, the third case refers to an air gap of 0.229 cm, and the pressure profile in the acceptor TNT is given in Figure 7. The $p^2\tau$ integral, evaluated for 2.31 usec, is 2190 kbar 2 -usec, and the peak pressure achieved was 119 kbar. The above results are also given in Table 5.

TABLE 5. DIMENSIONS OF MODELS AND RESULTS

CASE	PBX-9404 RADIUS cm	FIRST SHELL	THICKNESS FIRST SHELL cm	GAP cm	PEAK PRESSURE mbar	$\int p^2 dt$ kbar 2 usec	FIGURE
1	0.965	ALUMINUM	0.1016	0.0	100	2780	5
2	0.965	ALUMINUM	0.1016	0.051	111	2580	6.
3	0.965	ALUMINUM	0.1016	0.229	119	2190	7
4	1.120	ALUMINUM	0.1016	0.1143	127	3771	8
5	1.270	ALUMINUM	0.1016	0.1143	143	4575	9
6	0.863	ALUMINUM	0.2032	0.1143	65	1590	10
7	0.965	STEEL	0.1016	0.1143	98	2020	11
8	0.965	ZINC	0.1016	0.1143	81	1980	12

Note: Outer shell is aluminum in all cases with thickness of 0.127 cm.

Observe that as the air gap increases in size, the peak pressure experienced by the TNT acceptor increases, whereas the integral of $p^2\tau$ goes down. The increase in peak pressure is explained by the fact that the booster cup acts as a flying plate to generate the shock in the explosive when there is an air gap. The larger air gaps allow the detonation product gases to

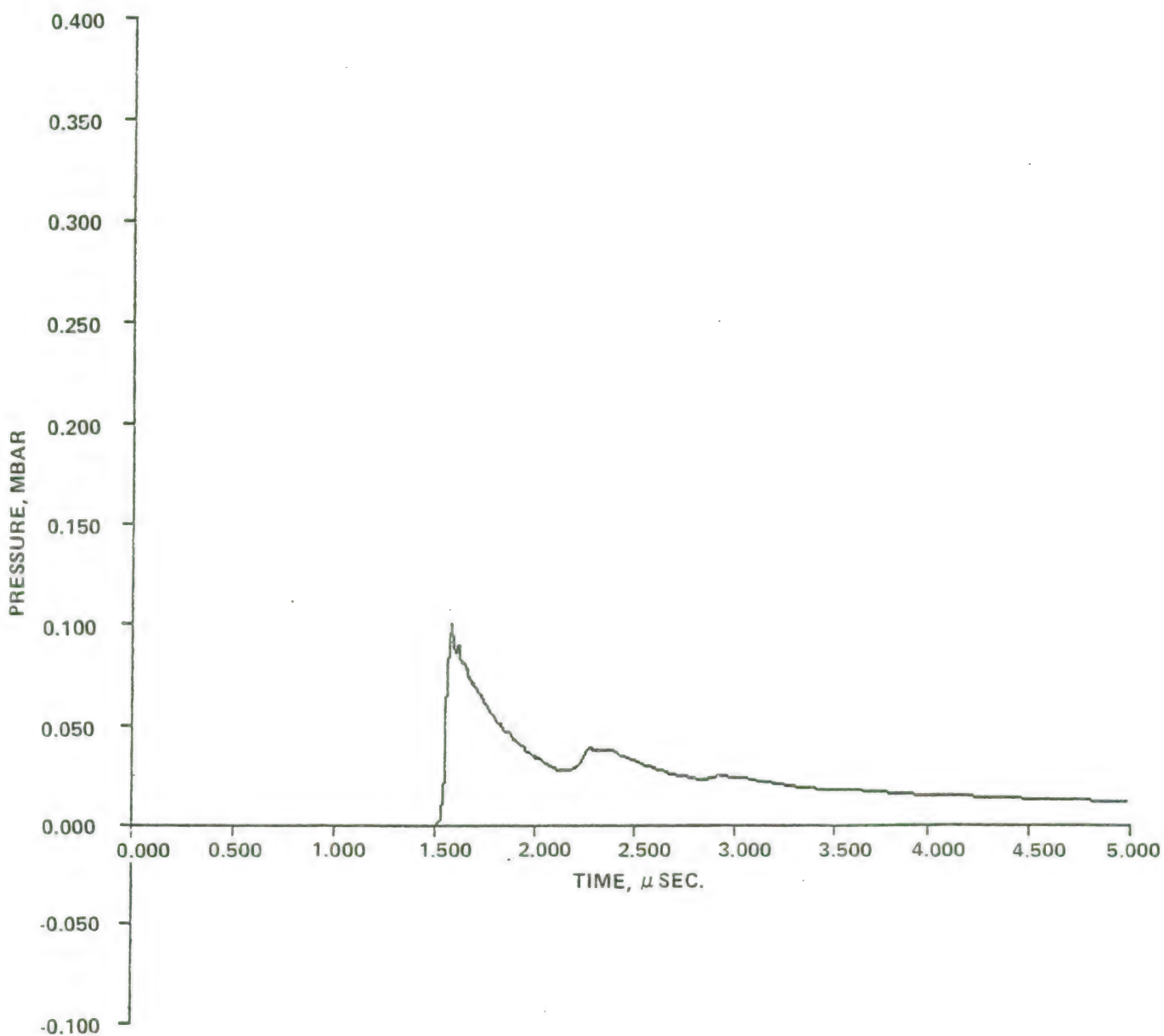


FIGURE 5. CASE 1, NO AIR GAP

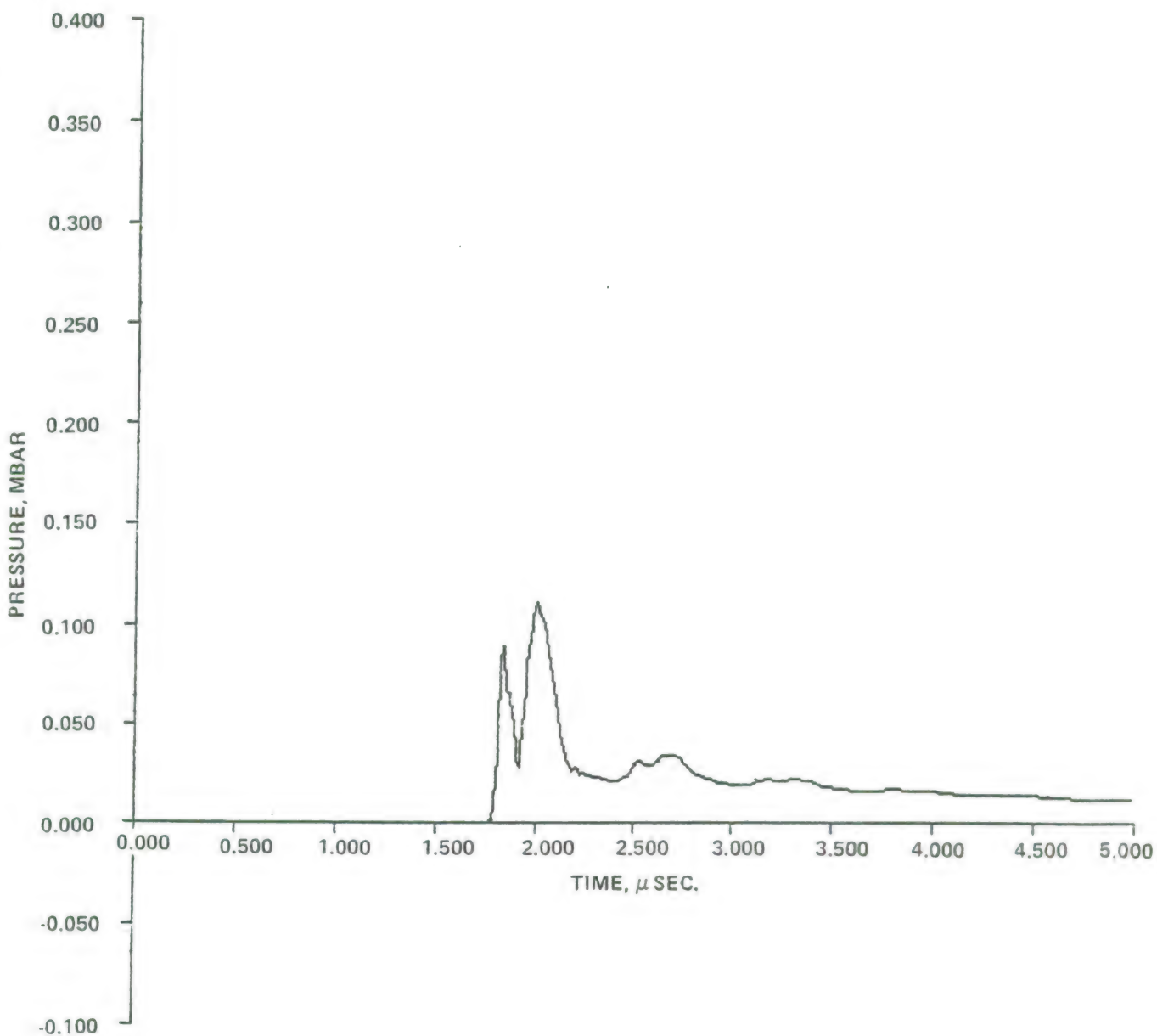


FIGURE 6. CASE 2, AIR GAP = 0.051 CM

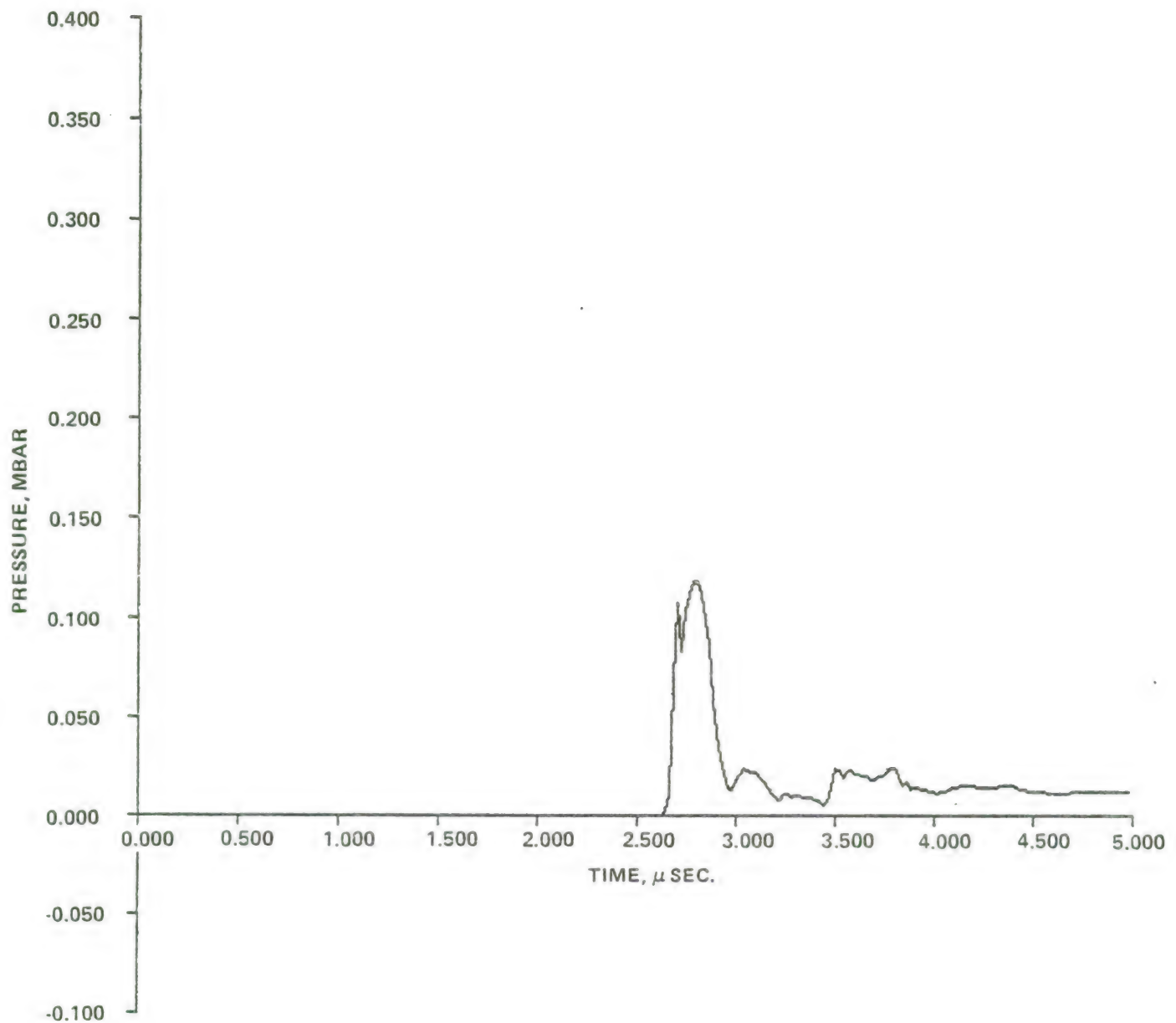


FIGURE 7. CASE 3, AIR GAP = 0.229 CM

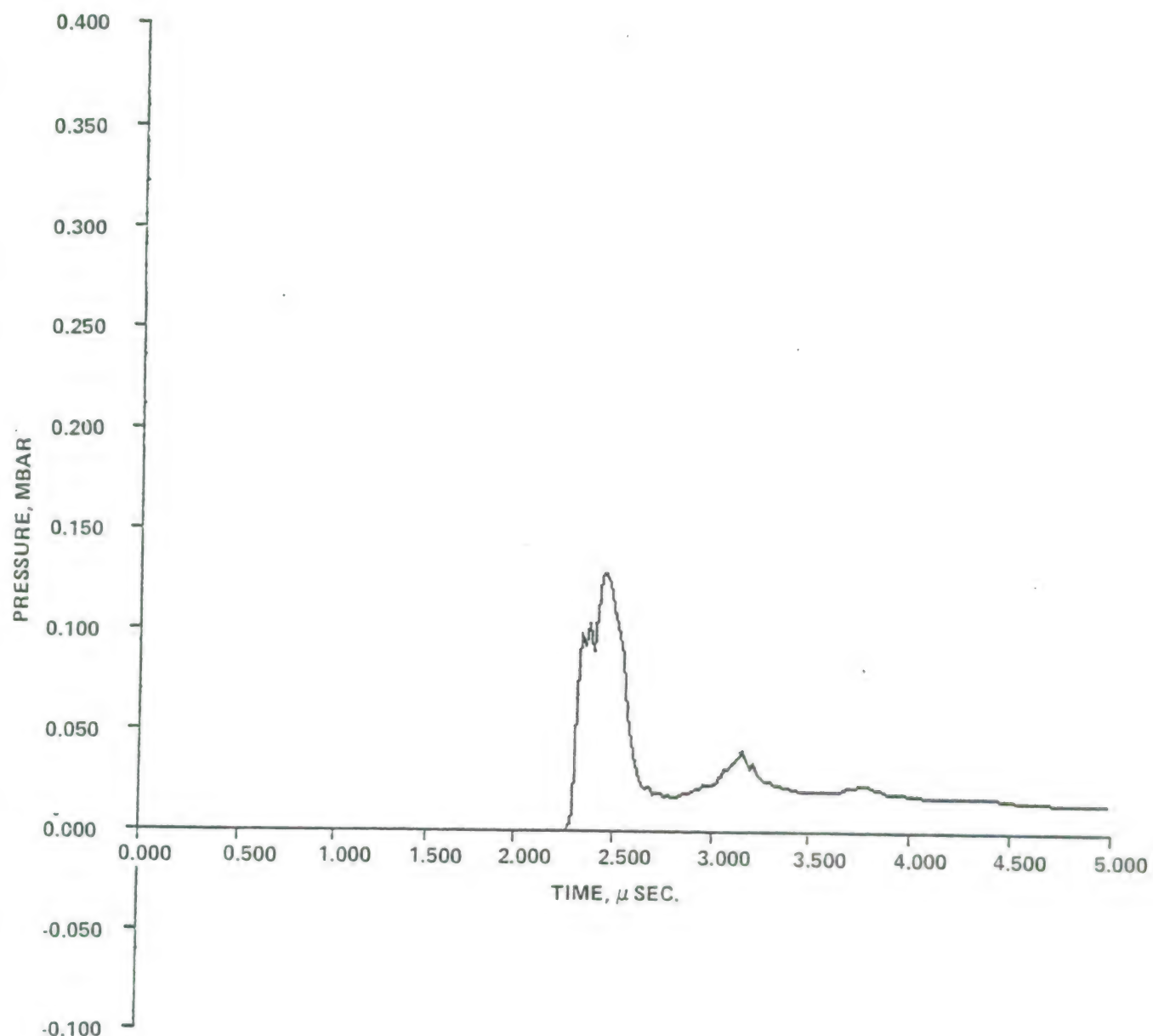


FIGURE 8. CASE 4, HEAD HEIGHT = 1.12 CM

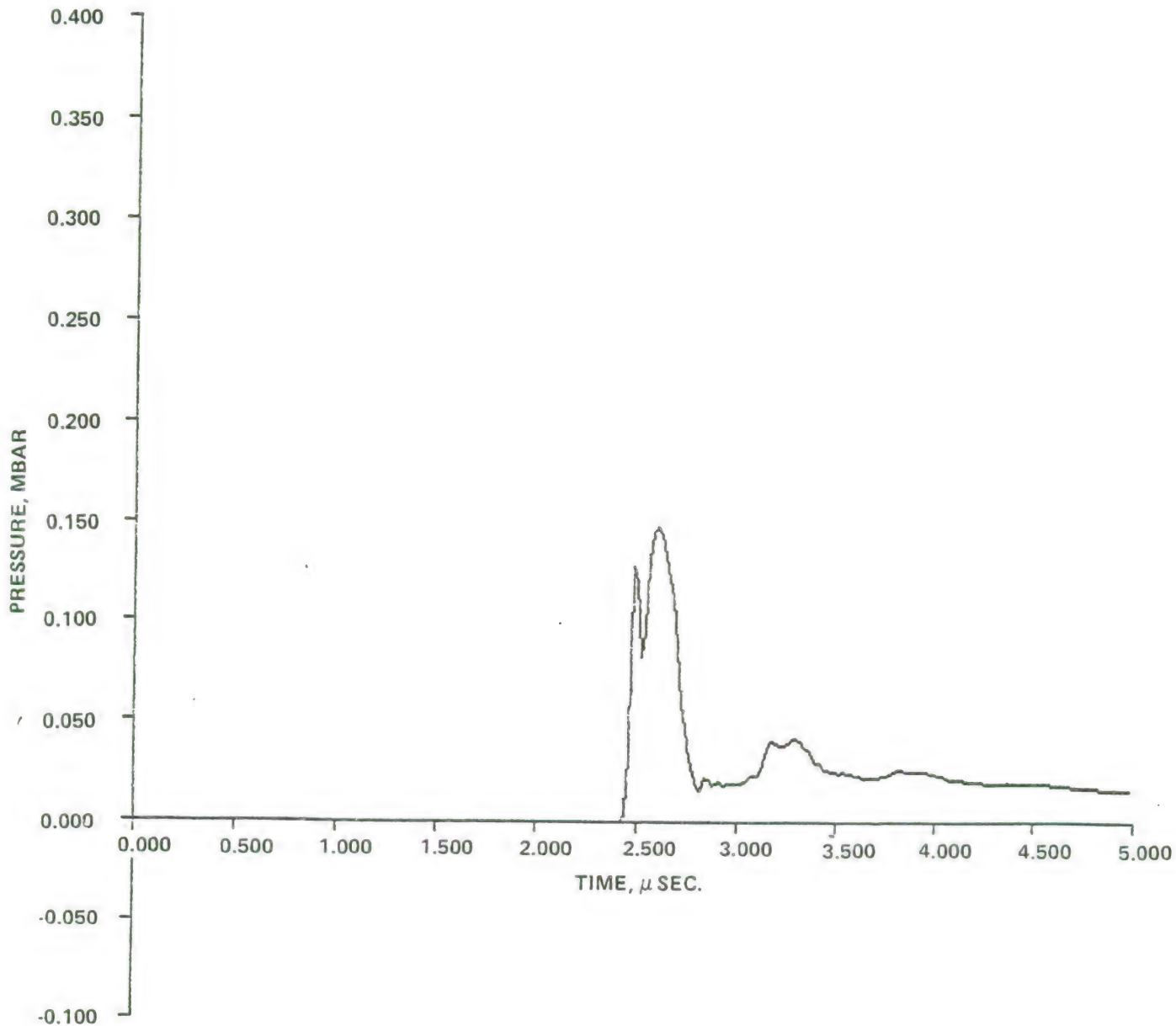


FIGURE 9. CASE 5, HEAD HEIGHT = 1.27 CM

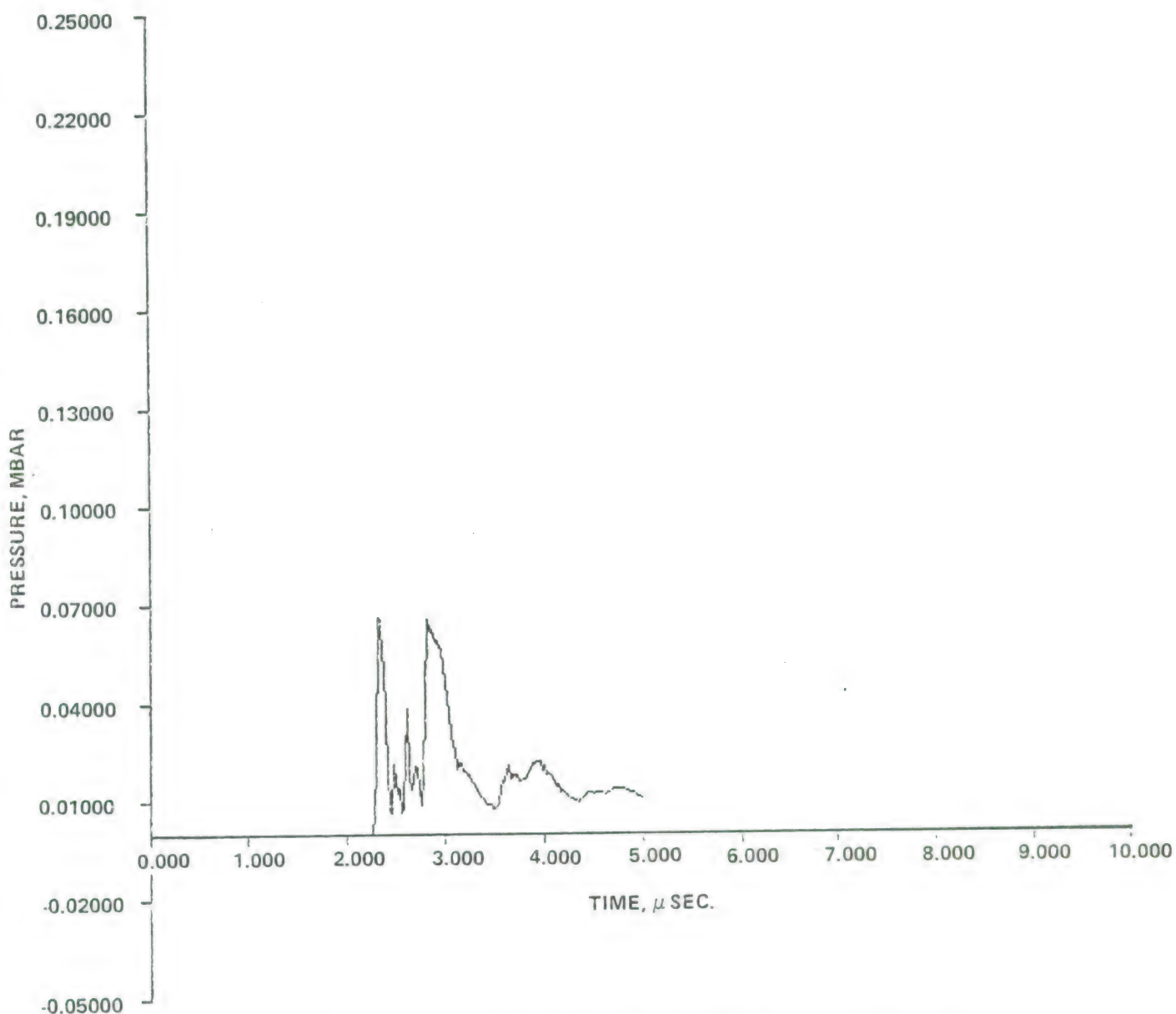


FIGURE 10. CASE 6, ALUMINUM BOOSTER CUP THICKNESS = 0.2032 CM

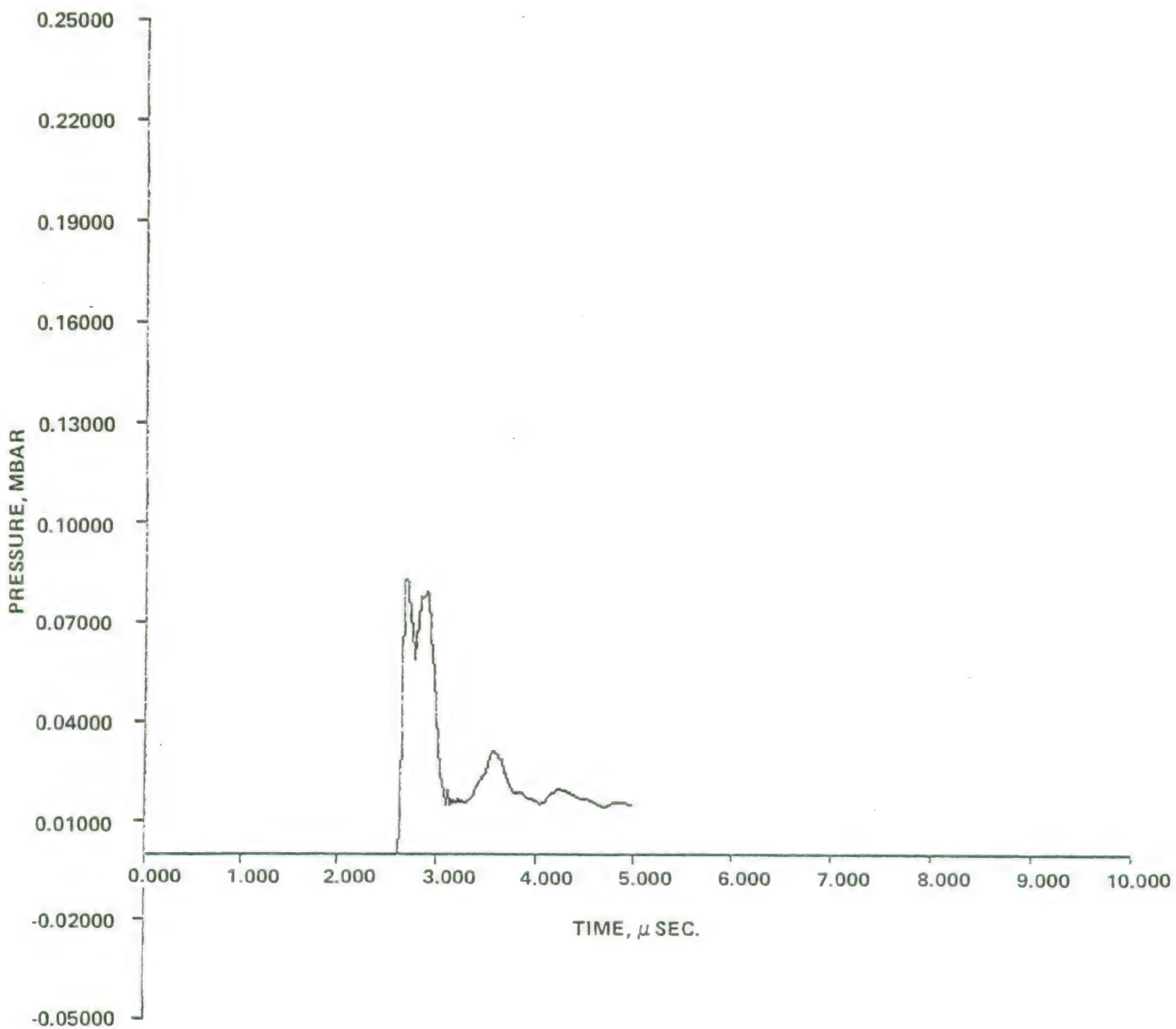


FIGURE 11. CASE 7, STAINLESS STEEL BOOSTER CUP

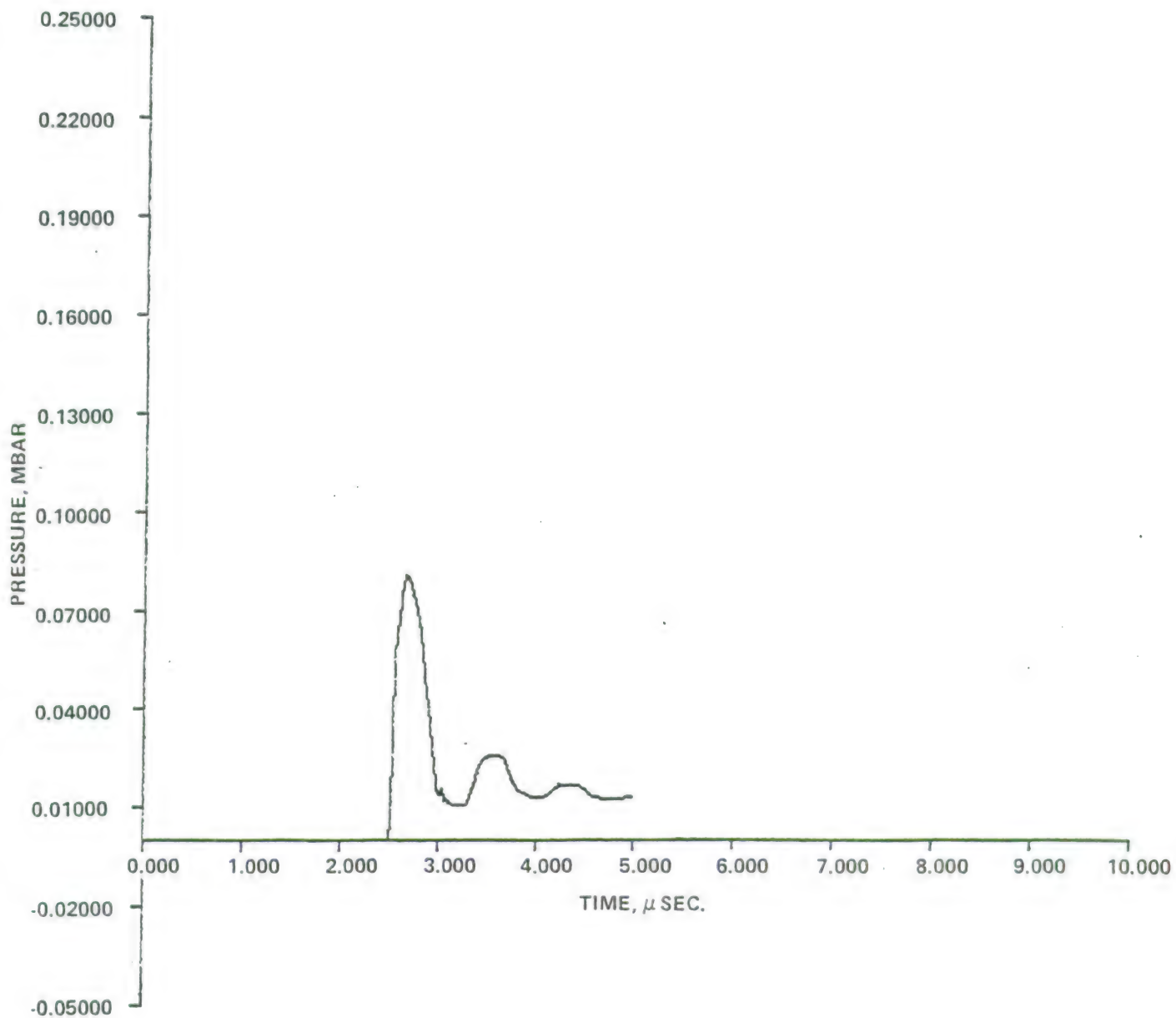


FIGURE 12. CASE 8, ZINC BOOSTER CUP

accelerate the flyer plate for a longer time so that it impacts the exploder well with greater velocity, thus producing a larger pressure peak. At the same time, the combustion gases expand to a lower pressure for the longer travel times, resulting in a stronger rarefaction being reflected from the back side of the booster cup into the acceptor. This results in a narrower peak and, therefore, a smaller value of $\int p^2 dt$. If $\int p^2 dt > (p^2 \tau)_{crit}$ is accepted as the proper criterion for detonation, then it is clear that the optimum situation is that of zero air gap. If, on the other hand, peak pressure is regarded as the proper criterion, then there will be some optimum non-zero air gap, larger than or equal to 0.229 cm. The true criterion is probably some combination of the peak pressure and $p^2 \tau$ quantity. In any case, it is noteworthy that for all three computations the resultant integrated $p^2 \tau$ values are larger than the critical values given in the Table 3 for fine TNT pressed to 1.55 g/cm³.

There is some uncertainty in determining $p^2 \tau$ values, since it is not clear over what time interval the integration should be taken. It is sometimes argued that the integration should be carried out only over the main pressure peak. If this is done for the third case, for example, then the $p^2 \tau$ value becomes 1842 kbar²-usec, still larger than the critical value of 324. Since the third case possesses the smallest $p^2 \tau$ integral, it seems clear that the first two cases also satisfy the initiation condition, even if the $p^2 \tau$ integral is evaluated only over the main peak.

Also investigated computationally was the effect of head height on the shock experienced by the acceptor TNT. The head height is defined as the thickness of booster explosive present in a given configuration. In the spherical computations, the head height corresponds to the radius of the outer boundary of the booster explosive (see Column 2 in Table 5). Consider, for example, case 4 in which the head height was taken to be 1.12 cm; the aluminum booster cup had thickness 0.102 cm, the air gap was 0.114 cm, and the aluminum exploder well had thickness 0.127 cm. The integral of $p^2 \tau$ is computed from the pressure pulse shape at a point in the TNT acceptor adjacent to the exploder well (see Figure 8), over an interval of 2.75 usecs. This integral has the value 3771 kbar²-usec. This is well over the critical $p^2 \tau$ value for initiation of TNT. It can be seen from Figure 8 that this main pulse had a duration of 0.47 usecs. If the $p^2 \tau$ integral is calculated just over the main pulse, its value is 2678 kbar²-usec. Again this exceeds the critical values given in this table. Note that the peak pressure for this pulse is equal to 127 kbars.

In the second run (case 5), the head height was increased to 1.27 cm, all other parameters remaining the same. The pressure profile in the TNT is shown in Figure 9. Calculated over an interval of 2.54 usecs, the $p^2 \tau$ integral equals 4570 kbar²-usec. The main peak is found to be 3406 kbar²-usec. The peak pressure equals 143 kbars.

It was found that increasing the head height increases both the $p^2 \tau$ integral and the peak pressure, while leaving the width of the main peak virtually unchanged.

Another variation of the configuration involved increasing the thickness of the aluminum booster cup, which required an equivalent decrease in the head height. The parameters of this run (case 6) are: head height (0.8634 cm),

aluminum booster cup thickness (0.203 cm), and exploder well, also aluminum (0.127 cm thick). A plot of the pressure versus time profile in the TNT acceptor adjacent to the explosive well is given in Figure 10. The peak pressure is 65 kbars, and the $p^2\tau$ integral, calculated over the duration of the profile (2.68 μ sec) is 1595 $\text{kbar}^2\text{-}\mu\text{sec}$.

The peak pressure has been considerably reduced. If the $p^2\tau$ integral is calculated only over the second peak, which is the thicker of the two peaks the value is 888 $\text{kbar}^2\text{-}\mu\text{sec}$. This lies within a factor of two of the critical $p^2\tau$ value.

DISCUSSION

A series of experimental trials designed to test the effect of various design modifications of the M732 fuze interface in 3"/50 projectiles has been reported in NSWC TR 82-20.¹ Although the computations do not exactly simulate the experimental test setups, they are sufficiently close to serve as representative examples of the behavior to be expected. Based on a $p^2\tau$ criterion for TNT, the computations tend to show that the acceptor explosive should detonate, whereas the experiments indicate that there are several configurations in which the detonation is low order. Table 1 of Reference 1 notes that shots 6 and 7 achieved high-order detonation. The distinguishing feature of these shots is that the booster pellet diameter has been increased to 3.17 cm; for the other shots, this value was 2.21 cm. This suggests that the critical factor to be considered is the failure diameter of the TNT, since the detonation transfer will be inhibited if the diameter of the booster pellet is less than the failure diameter of the acceptor. The computations do not take this failure diameter into account, so that a successful detonation transfer is predicted. The experiment achieved successful transfer when the pellet diameter was increased; therefore, it may be concluded that the results are consistent with the experimental observations and with the hypothesis that the failure diameter of the TNT is the limiting factor in the detonation transfer from the M732 fuze in the 3"/50 projectile.

The $p^2\tau$ values for the first three entries in Table 5 decrease as the air gap is increased, while the peak pressure also increases. This leads to the conclusion that the air gap should be made as small as possible. Increasing the head height increased both the peak pressure and the values of $p^2\tau$. This is not surprising, of course, with more explosive pushing the same mass of metal (see cases 4, 5, and 6 in Table 5).

The seventh entry in Table 5 is for a stainless steel cup. This case gives a smaller peak pressure and a smaller value for $p^2\tau$ than did the first five entries in Table 5 with the same head height. This case will be discussed more fully in Appendix A.

The last entry in Table 5 shows that the use of zinc in the booster cup is about the same as in the steel ring.

REFERENCES

1. Montesi, L. J., Fuze M732 Boostering of Cast TNT Loaded 3"/50 Projectiles, Phase I: Exploratory Tests and Results (Apr - Jun 1981), NSWC TR 82-20, 30 Jun 1982.
2. Lawrence, R. J., and Mason, D. S., Wondy IV - A Computer Program for One-Dimensional Wave Propagation with Rezoning, SC-RR-284, Sandia Laboratory, Aug 1971.
3. Kinslow, Ray, High-Velocity Impact Phenomena (New York: Academic Press, 1970).
4. Coleburn, N. L., and Liddard, T. P., Jr., "The Unreacted Hugoniot Equation-of-State of Several Explosives," J. Chem. Phys., Vol. 44, 1966, p. 1929.
5. Lawrence, R. J., Mason D. S., and Benzley, S. E., Dynamic Material Property Library, SC-DR-68-885, Sandia Laboratories, Dec 1968.
6. McQueen, R. G., and Marsh, S. P. "Equation of State for Nineteen Metallic Elements from Shock-Wave Measurements to Two Negabars," J. Applied Phys., Vol. 31, 1960, p. 1253.
7. Wilkins, Mark L., Calculations of Elastic Plastic Flow, Lawrence Radiation Laboratory, UCRL-7322, Rev. 1.
8. Dobratz, B. M., LLNL Explosive Handbook, Lawrence Livermore National Laboratory, UCRL-52997, 16 Mar 1981.
9. Hubbard, H. W., and Johnson, M. H., J. Applied Phys., Vol. 30, 1959, p. 765.
10. Walker, F. E., and Wasley, R. J., Critical Energy for Shock Initiation of Heterogeneous Explosives, Explosivestoffe, Vol. 17, No. 9, 1969.
11. Taylor, B. C., and Erwin, Separation of Ignition and Buildup to Detonation In Pressed TNT, Sixth Symposium (International) on Detonation, ACR-221 Office of Naval Research, Department of the Navy, 24-27 Aug 1976.

APPENDIX A

COMMENTS ON THE INTERACTION OF WAVES IN A SPHERICAL MODEL OF A BOOSTER

INTRODUCTION

The configuration of a booster/main charge system is described in the main text of this report. That system is simulated on a computer as a spherical system. This permits the use of a code for flow in one dimension. More accurate results would be obtained by using a code for two-dimensional flow. The cost of such a computation is much greater than that for the computation for one-dimensional flow. It was decided that the costs for doing the two-dimensional calculations were not justified, and that the results of the one-dimensional calculations would reveal the salient features of the flow.^{A-1} In this appendix a detailed description of the results for a particular spherically symmetric computer run for a problem involving a steel booster cup is presented. The shock transmissions and wave reflections occurring at various times and places are analyzed, and plots of the variations of parameters with time and space are also given.

INITIAL ACCELERATION OF THE SIMULATED BOOSTER CUP

A considerable amount of insight into the behavior of pressure wave propagation and interaction in the booster can be obtained from a spherical computer model. The booster charge is modeled as a sphere detonated at its center and is contained in a spherical shell of stainless steel. The booster well is a spherical aluminum shell. The two shells are separated by a void. The main charge is in contact with the entire surface of the outside of the aluminum shell. For this problem the head height is 0.965 cm, the thickness of the steel booster cup is 0.102 cm, the void is 0.114 cm, and the thickness of aluminum exploder well is 0.127 cm (see Figure A-1 for further clarification). Having the booster described in spherical coordinates permits the use of a code which solves the flow equations in one dimension. The code used for this work was obtained from Sandia National Laboratory and is called WONDY IV.^{A-2}

The code output of interest to the warhead designer is the amplitude and duration of the shock wave system induced in the main charge (TNT). The code can be used as a design aid by manipulating the thickness of one or more of the materials to get an indication of how these changes affect the shock wave entering the main charge. This should give the designer a useful tool for designing booster system, and should result in lowering of the cost of booster design.

The main object of this section of the report is to show how the detonation wave, shocks and pressure waves, and relief (rarefaction) waves propagate through the spherical model of the booster. These waves interact with each other, and they interact with interfaces between materials. These interactions would show up much more clearly if the problem was solved by the method of characteristics. Codes based on the method of characteristics are difficult to program for a computer. For practical reasons, i.e., lower cost and faster turnaround, codes employing "artificial viscosity" are commonly used. These codes spread out discontinuities so that the equations which describe continuous flow can be used across discontinuities. These codes are referred to as "artificial viscosity codes," "Q codes" or "hydrocodes." Information can be extracted from the output of such codes so that wave diagrams can be drawn. These diagrams then serve as a guide for understanding the flow in the booster/main charge system. Thus, we get most of the useful results that we would have obtained from a method of characteristic solution.

Figure A-2 shows nine streamlines (also called particle paths), eight of which are labeled L1 through L8. Note that the fifth line from the bottom is labeled L4A. This streamline merges with L4 when the gap closes. Observing L1, we see that the detonation front, which started at the origin, arrived at about 0.61 μ sec causing a discontinuity in the slope of the streamline. Immediately after the arrival of the detonation front, the particle begins to slow down--the slope of the particle path L1 decreases. This takes place because of the Taylor wave that is described in the literature as a simple centered relief wave. It is centered at (0,0), the same point at which the explosive was detonated.

At 1.12 μ sec, the slope of L1 becomes zero, signifying the end of the Taylor wave. For the next 1.04 μ sec, path L1 has zero slope. This is as it should be for a spherical detonation wave.

For streamline L2, the wave system is similar to that of L1. The detonation front arrives a little later (at 0.94 μ sec) (see points A1 and A2 in Figure A-2). The first element of the Taylor wave--whose pressure is 160 kbar--arrives at L2 at 1.56 μ sec. The reason for this is the divergence of the Taylor wave fan. For L2 the duration of the zero slope part of the particle path is only 0.10 μ sec (see point B2). This shorter duration is due to a wave reflected from the explosive/steel interface, point A3. It intersects path L2 at point C2 and causes the velocity to become negative.

The pressure for paths L1 and L2 are given in Figures A-3 and A-4 along with their X,T curves. One of the important things shown in these plots is the steep decrease of the pressure following the shock front peak. At 1.12 μ sec, the pressure becomes constant in Figure A-3, but not zero. The rise in pressure at 2.2 μ sec is due to a shock that results from the interaction of the detonation front with the gas/steel boundary, point A3 in Figure A-2. Comparison of Figures A-3 and A-4 shows that this shock was moving to the left--it is described as being a backward facing shock. This shock interacts with the Taylor wave in the detonation product gases. The pressure relief following this backward facing shock shows some ripples. These may be artifacts of the computer code. Q-codes cannot give accurate results near discontinuities, such as a shock front, because they use the equations for smooth flow and require the use of an artificial viscosity in order to take care of shocks. They can, however, give the salient features of the flow which are needed.

Note that the peak pressure in Figure A-4 is greater than that in Figure A-3. This is undoubtedly due to the inability of the Q-code to adequately treat the flow in places where pressure gradients are great. A finer grid could be used if more detail was desired.

Figures A-5 and A-6 show the particle velocity and the X,T curves for streamlines L1 and L2. These plots are useful for finding the locations of the interactions of waves with one another and with interfaces the X,T plots. An abrupt change in the particle velocity means that there is an abrupt change in slope in the particle path. The detonation front reaches the explosive/steel interface at $T = 1.5 \mu\text{sec}$ (see point A3 in Figure A-2). There results the transmitted shock (see the line drawn between points A3 and A4 and the reflected shock as described above). At point A4, which is on the free surface of the steel, the shock is reflected as a relief wave which moves backward in the steel and on into the gases at point A5. It is this strong rarefaction that overtakes the backward facing shock and attenuates it. The data necessary to construct these interactions accurately are not available.

More or less abrupt changes can be detected in the slope of streamlines L3 and L4 in Figure A-2. The first, at point A5, has already been addressed. Other points on L3 are labeled I, J, K, and L. The second break in slope of L4 in Figure A-2 is labeled A6. The locations of these breaks correspond to abrupt changes in the particle velocities (see Figure A-14). The problem now is to determine the origin of waves causing these breaks in slope. The break at point I accelerates L3, so it could be caused by a shock wave coming out of the gas. Or, it could be a rearward facing rarefaction arriving from the free surface of the steel, streamline L4. The latter seems most likely. At J, the streamline L3 is accelerated again. Using the same argument as above, it can be deduced that a rarefaction must have arrived from the free surface (L4) of the shell. The only detectable change in the slope of L4 is at the point A7. It must be caused by the arrival of a shock wave which originated on the other side of the steel plate. It may be, of course, the result of wave interaction in the steel plate, such as would happen if the plate fractured. For more detail, look at Figure A-9 and Figure A-15. These two figures make it easier to locate changes in slope of L4 in Figure A-2.

The changes in slope mentioned above are probably caused by reflection of the wave at A5. Ringing is possible--it consists of repeated reflections of waves in a layer of material with certain boundary conditions. Here the steel has a greater acoustic impedance than the gases and, of course, the void. So relief waves are reflected as compression waves, and vice versa, at the surfaces of the steel. Here the steel is 0.101 cm thick, so assuming an average wave velocity of $0.5 \text{ cm}/\mu\text{sec}$, a reverberation (across and back) should take $(2.0 \times 0.102)/0.5 = 0.4 \mu\text{sec}$. The dashed lines, the first through points A5 and A6, the second through points A6 and to the vicinity of point J, represent such a system of waves in Figure A-2. Symbols c and r are for compression and relief waves, respectively. But events at I and A7 are not explained by this ringing model. There appears to be some other phenomenon affecting the motion of the surface of the steel. A more thorough examination of the computed results will show the nature of this phenomenon.

SOME RULES GOVERNING WAVE PROPAGATION AND INTERACTIONS

Before continuing the discussion of the movement of the steel shell, it will be useful to state some of the rules governing wave propagation and interactions. Waves may interact with each other, with discontinuities such as that at interfaces between two materials of different densities, and with free surfaces. A property of materials called the acoustic impedance governs the way waves interact at interfaces. The acoustic impedance is the product of the density, ρ , of the material, and its sound speed, c . When a compressive wave in a material with a relatively large value of ρc comes to an interface with a low impedance material, the wave reflects back into the high impedance material as a rarefaction or rarefaction wave. If the compressive wave approaches the interface from the low impedance side, it will be reflected as a compression wave. A free surface may be regarded as a material with 0.0 impedance. Because ρc is less in the gas than in the steel, the detonation front reflects at point A3 (see Figure A-2) as a shock wave. Because this reflected shock is moving to the left, it is described as a left-facing or backward-facing wave. Similarly, the detonation front and the Taylor wave elements are said to be forward-facing waves. These concepts may be clarified by examining Figures A-3 and A-4 again. Note that in Figures A-5 and A-6, the particle velocity increases for forward-facing waves, and decreases for left-facing waves. In the present example, the particle velocities become negative after the left-facing shock.

The equations governing high pressure flow are so difficult to solve that we have to use finite difference methods. But, it is the methodology of the method of characteristics^{A-3} that helps us understand what goes on. That method is based on the assumption that both rarefaction waves and compression waves can be represented by a series of low amplitude waves that we call "wavelets." In the X,T space, each wavelet is represented by a line ("curve" would be more appropriate if we had details of the flow) that we call an "element" of the wave. If all these lines, i.e., elements, originate at a common point, the wave is said to be a centered wave. The set of diverging lines may be called a "fan." In the present problem, the Taylor wave is centered at the center of the sphere of the explosive. In Figure A-2, the Taylor wave is represented by the thin lines which diverge slightly from the solid line representing the detonation front. The spacing of these lines is obtained from Figures A-3 and A-4 which give the pressure versus time along streamlines L1 and L2. The change of pressure to the immediate right of the detonation front is so rapid, it is difficult to draw elements of the wave carrying pressures near that of the detonation front. Hence, we start by showing the 160 kbar element. Other elements are as shown in Figure A-2. The increments in pressure were chosen arbitrarily for convenient spacing in the plot. At the surface, each of these elements causes an element to be reflected into the gases, and an element traveling into the steel. These latter elements are not shown in Figures A-2 and A-7 because of lack of space. The reader must realize, however, that these wavelets are important in solving the problem in detail.

A property of high pressure flow involving shocks is that a rarefaction following a shock overtakes the shock and attenuates it. In the present problem, we have the rarefaction fan centered at point A4 following the shock originating at point A3 (see Figure A-2). The interaction of these two waves reduces the amplitude of the reflected shock in the gases. These interactions account for the decrease in pressure following the second maximum in the curves in Figures A-3 and A-4.

The reflection of the shock at point A4 (see Figure A-2) gives rise to a simple centered rarefaction wave; therefore, the reflected wave should be represented by a fan, not by the single line connecting points A⁴ and A5 in Figure A-2. Each element of the fan yields an element transmitted into the gases, and a reflected compressive element. These elements interact with the elements of the Taylor wave, both those in the gases and those elements that are transmitted into the steel. In the steel, these rarefactions, which should be represented by fans of elements, are oriented so that their interactions produce negative pressures, i.e., tension in the steel shell. This process may produce tensions that overcome the strength of the material, causing it to fracture. This process is called "spalling" or "scabbing." The effect of spalling on the model booster will be pursued in the following section.

Again, lack of space prohibits the inclusion of all the elements of the rarefaction waves and compressive waves. The serious reader should make sketches as an aid in understanding what has been given above and, perhaps, try to add more waves and wavelets.

EFFECTS OF SPALLING IN THE STEEL SHELL

Figure A-7 is an enlargement of a portion of Figure A-2. Points and streamlines are labeled as they are in Figure A-2. Before reading further, however, one should first examine Figures A-8 through A-19. Figures A-8 through A-13 each show both the appropriate P,T curve for a given streamline and the streamline--the X,T curve. Similarly, Figures A-14 through A-19 show the particle velocity curves and the appropriate X,T curves. It is not possible to explain all the features of these curves, however, because some features may be due to the method used to solve the differential equations which describe the flow. Some of the features are due to spalling that will be explained in some detail in the following.

As was noted above, when two rarefactions of the proper orientation interact in a solid, the pressure may become negative, i.e., the material is in tension. In the steel, we have the rarefaction wave centered at the point A4 in Figure A-7, interacting with the elements created by the impingement of the Taylor wave elements on the interface. Elements of these two rarefactions are not shown in Figure A-7 because of the small scale. The tensions may exceed the strength of the material so that it fractures, or spalls.^{A-4} Spall strength is difficult to measure, partly because the process takes place so quickly, and partly because spall strength is poorly defined. For example, only hairline fractures may be observed when a piece of shocked material is sectioned and examined microscopically. In other cases, the specimen may come apart, leaving two pieces which may have no attachment at all. Values of the spall strength for a few materials are given by Davison and Graham.^{A-5} For the work reported here, -50.0 kilobars was used as the spall strength of the steel, and -25.0 for the aluminum.

When the pressure falls below the value chosen for the spall strength, the computer code creates a void and gives the X,T coordinates of the fracture. There are three such points in the steel in Figure A-7, F1, F2, and F3. At later times, the voids are closed because the explosive product gases are still pushing on the shell. The locations of the closing of the voids are also given in Figure A-7 (see points C1, C2, and C3). Points F1 and F2 must lie in the

region where the rarefaction wave centered at point A4 overlaps the Taylor wave centered at the detonation point. If this were not true, no tensions could be created and no spall would be produced. The separation labeled F3 is due to the reopening of the fracture labeled F1. Reopening is allowed to happen at -5.0 kbars by the code.

The X,T coordinates of the fractures and closures in the steel, as shown in Figure A-7, are tabulated in Table A-1.

TABLE A-1. LOCATIONS OF FRACTURES, CLOSURES AND SPALL TENSIONS

TIME μSEC	LOCATION CM	TENSION KBARS	TIME μSEC	LOCATION CM
1.50	1.04	53.0	--	--
1.05	1.02	50.0	--	--
--	--	--	1.74	1.04
1.91	1.06	5.5	--	--
--	--	--	2.14	1.08
--	--	--	2.23	1.12

When the steel spalls, the material at the new free surfaces is no longer under stress. In order for this to happen, shock waves are created at the point of fracture. Their amplitudes are governed by the spall strength, -50.0 kbar in the steel. If a fracture is closed due to wave interaction, it may later reopen. The stress at which this can take place is -5.0 kbar.

Both surfaces of the steel, represented by streamlines L3 and L4, should be affected by the pressure waves created by spalling at points F1 in Figure A-7. The free surface is surprisingly unperturbed until the time is 2.35 μsec (see point A7, Figure A-2). Examination of Figure A-15, however, shows that the particle velocity of L4 has a damped oscillatory component. The amplitudes of these oscillations are too small to affect the particle path L4 by a detectable amount. The period of the oscillation is 0.014/μsec. The points F1 and C1 in Figure A-7 are 0.034 cm from the free surface. Using the value of 0.5 cm/μsec for the average wave speed, it takes a wave $0.034/0.5 = 0.068$ μsec for a one-way trip through the spalled piece of steel. A round trip then takes 0.136 μsec. This is essentially the value of the period determined above for the oscillation superimposed on the particle velocity curve for streamline L4 in Figure A-15. From the agreement of the two values of the periods, it is deduced that the code is doing a good job of calculating some details of the flow in addition to giving the salient features of the flow.

On the original plot, there is a change in the slope of streamline L4 at point A7 in Figure A-7. This change could arise from the closure at point C1 of the fracture which occurred at point F1 (see Figure A-7). Closure of a void also creates compressive waves, in this case a shock wave. Such a shock should, after impinging on the as yet free surface, path L4, accelerate that path. Hence, the increase in particle velocity at point A7 appears to be caused by a shock from the neighborhood of point C1.

The backward traveling (toward the gas) shock also created at point F1, and which is not shown in Figure A-7, must affect the flow in the back side of the steel and the flow in the gas. This is also the case for the fractures at points F2 and F3 (the reopening of the fracture closed at C2) and the closures at C2 and C3. While the results from a detailed analysis of the effects of these waves would be interesting, it is probably not very important because it will have no effect of interest on the initial flow in the TNT, which is what we are after in this report. Scholars may try their hand at constructing a plausible X,T-diagram. The going gets rough because there are more than two-wave systems. Most of us prefer to accept the result of a well run reliable hydrocode. Some hints are given in Figures A-2 and A-7 by the dashed lines. The shock in the TNT is located at points Q, R, S, and T in Figure A-2. Backward facing shocks are generated at points P and Q, and are refracted into the gases at points L and M respectively. A forward facing shock is created at point M; it is reflected into the aluminum at point O as a rarefaction wave.

ON TO THE TNT

The steel shell closes the gap originally between it and the aluminum at 2.48 μ sec. This collision produces a forward facing shock in the aluminum, and a backward facing shock in the steel (see Figure A-2). At point Q, lying on the interface between the aluminum and the TNT, a rarefaction is created in the aluminum which travels back toward the steel. No reflections take place at the points R, S, and T in Figure A-2 because these points are in the TNT. The pressures for streamlines L5, L6, L7, and L8 are of interest to the warhead designer. The designer will want to know both the amplitude of the shock in the TNT and the duration of the pressure. These data are given in Figures A-8 through A-13. Many of the features of the pressure pulse have been wiped out, hopefully by the natural processes of wave interaction rather than by unwanted processes introduced by the computational method.

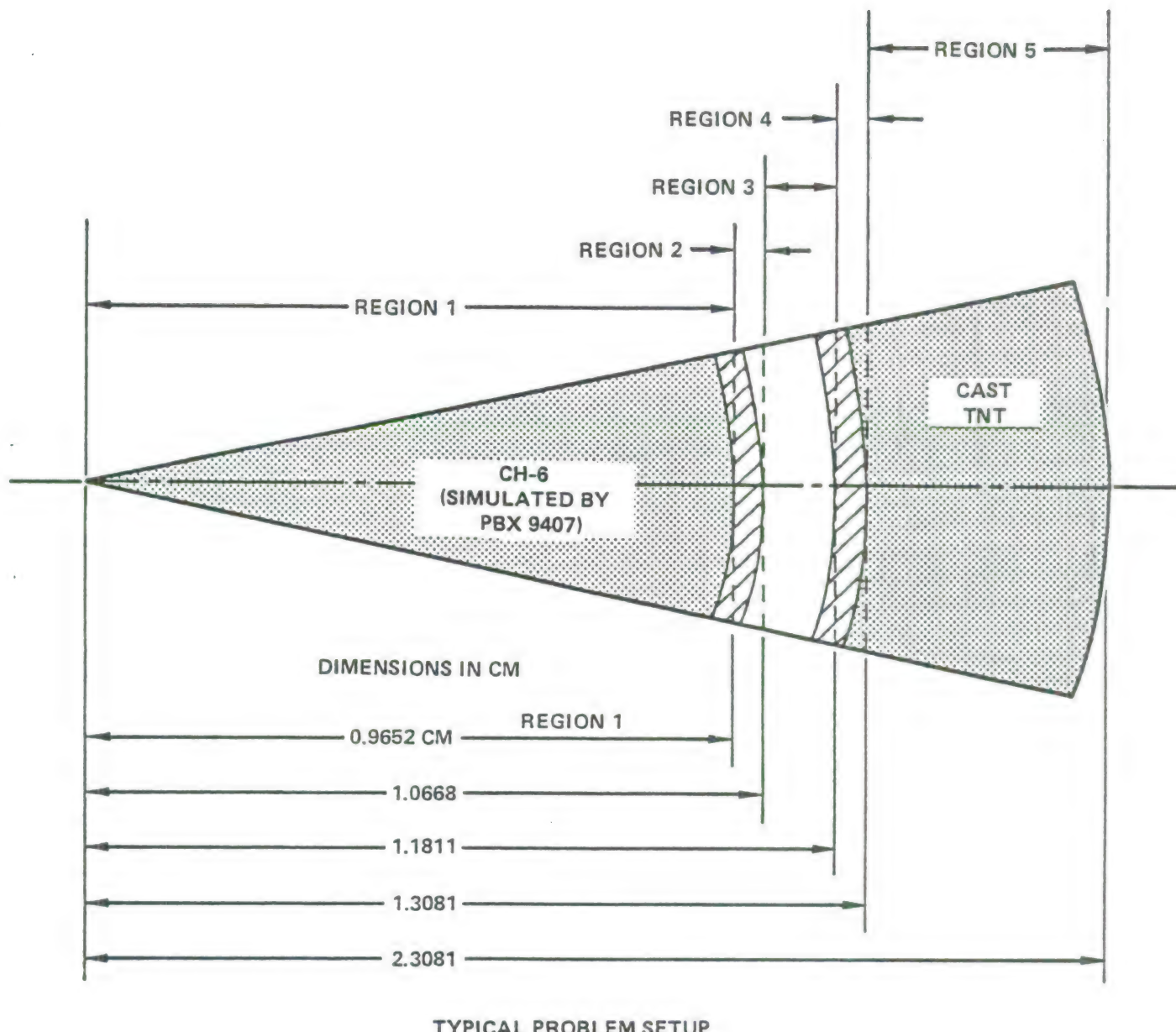
For comparison with tests such as the large scale gap test (LSGT),^{A-6} it would be better to use results given in Figure A-11 rather than those given in Figure A-10. This is recommended because of experience in using this code and others like it. The discontinuity in density at the interface causes the code to give some errors in its representation of the flow. Results given in Figure A-11 are for the streamline L5 which is 0.01 cm inside the TNT. An interpolation could be used to get a more representative value of the pressure at the interface.

The pressure spike at $t = 1.36 \mu$ sec in Figure A-9 may appear to the uninitiated as an anomaly. It occurs at the time at which the surface of the steel shell starts moving across the gap, point A4 in Figure A-7. The boundary condition at the free surface of the steel requires that the stress be zero. The code handles this boundary condition by making use of a virtual zone outside

the boundary. In the virtual zone, stress, density and pressure are initialized to zero at the start of the computations. The free surface velocity is obtained by solving the finite difference equations using the values of stress, density, etc., from the virtual zone, and from the last zone in the shell. The calculations also give the new values of pressure and density in the last zone of shell. The finite difference equations are designed to give the pressure in the middle of a cell. Hence, the pressure given in Figure A-9 is for a point a half-cell width inside the steel. From the zone width, 0.004 cm, the point for which the pressure reported in Figure A-9 applies is 0.002 cm from the free surface (neglecting compression). The duration of the pressure pulse, measured close to its base, is 0.06 μ sec. The round trip from the center of the cell to the free surface and back is 0.004 cm. Dividing the distance by the time gives 0.07 cm/ μ sec for wave velocity (shock going toward the free surface, a rarefaction coming back). This value of the velocity is almost an order of magnitude too small. This can be accounted for by taking the spreading of the shock front over up to 4 or 5 zones, and the natural spreading of the rarefaction front.

It is not claimed here that the solution being reported is completely accurate. This holds for the spalls and other features of the solution. Because of experience with other calculations and with experiments, it is considered to be very likely that spalls would take place in an experiment containing the components used in this computer modeling problem. It would be of interest to do some experiments which would test the validity of predictions of the code and, at the same time, perhaps convince warhead designers that their designs create wave interactions not anticipated.

The condition of the steel could be determined by a soft recovery--a difficult operation. Another method would be to let the steel hit a pressure sensitive gauge, e.g., Manganin. If the steel is separated into two or more pieces, the gauge would show the arrival of the first part, a drop in the pressure, and then the arrival of the shock created by the second or more piece(s) of steel.



TYPICAL PROBLEM SETUP

REGION	ZONE ALLOCATION	MATERIAL	REGION THICKNESS		ZONE THICKNESS CM
			CM	INCHES	
1	1 THROUGH 124	PBX 9407	0.9652	0.380	0.0078
2	125 THROUGH 151	ALUMINUM	0.1016	0.040	0.0040
3	VOID	AIR GAP	0.143	0.045	-
4	152 THROUGH 183	ALUMINUM	0.127	0.050	0.0042
5	184 THROUGH 283	TNT (NON-REACTIVE)	1.0	0.394	0.0100

FIGURE A-1. COMPUTATIONAL MODEL USED IN THE CODE FOR FLOW IN ONE-DIMENSION

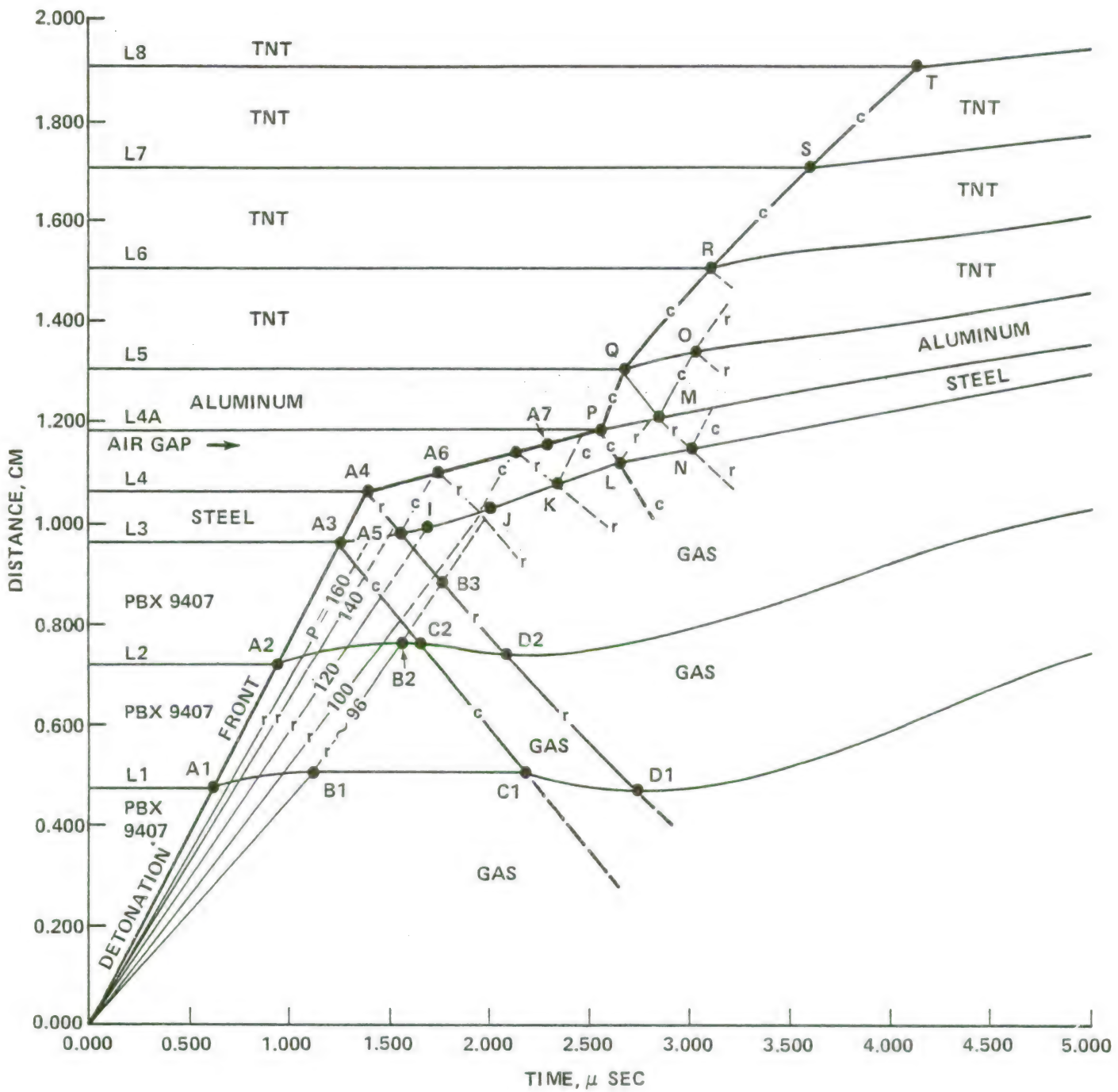


FIGURE A-2. DISTANCE VS TIME FOR WAVE INTERACTION IN COMPUTER MODEL OF BOOSTER

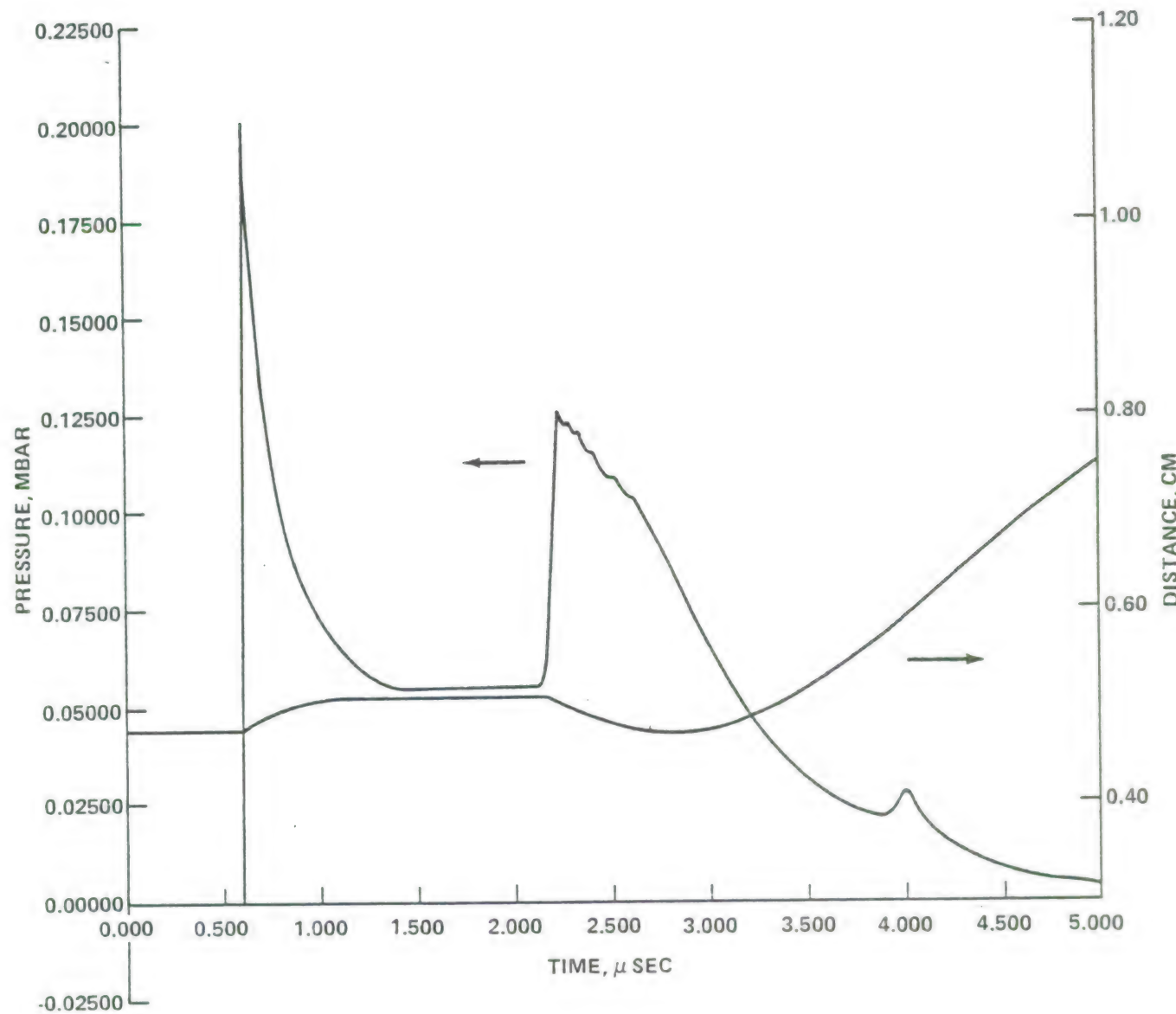


FIGURE A-3. PRESSURE AND DISTANCE VS TIME FOR PARTICLE PATH L1

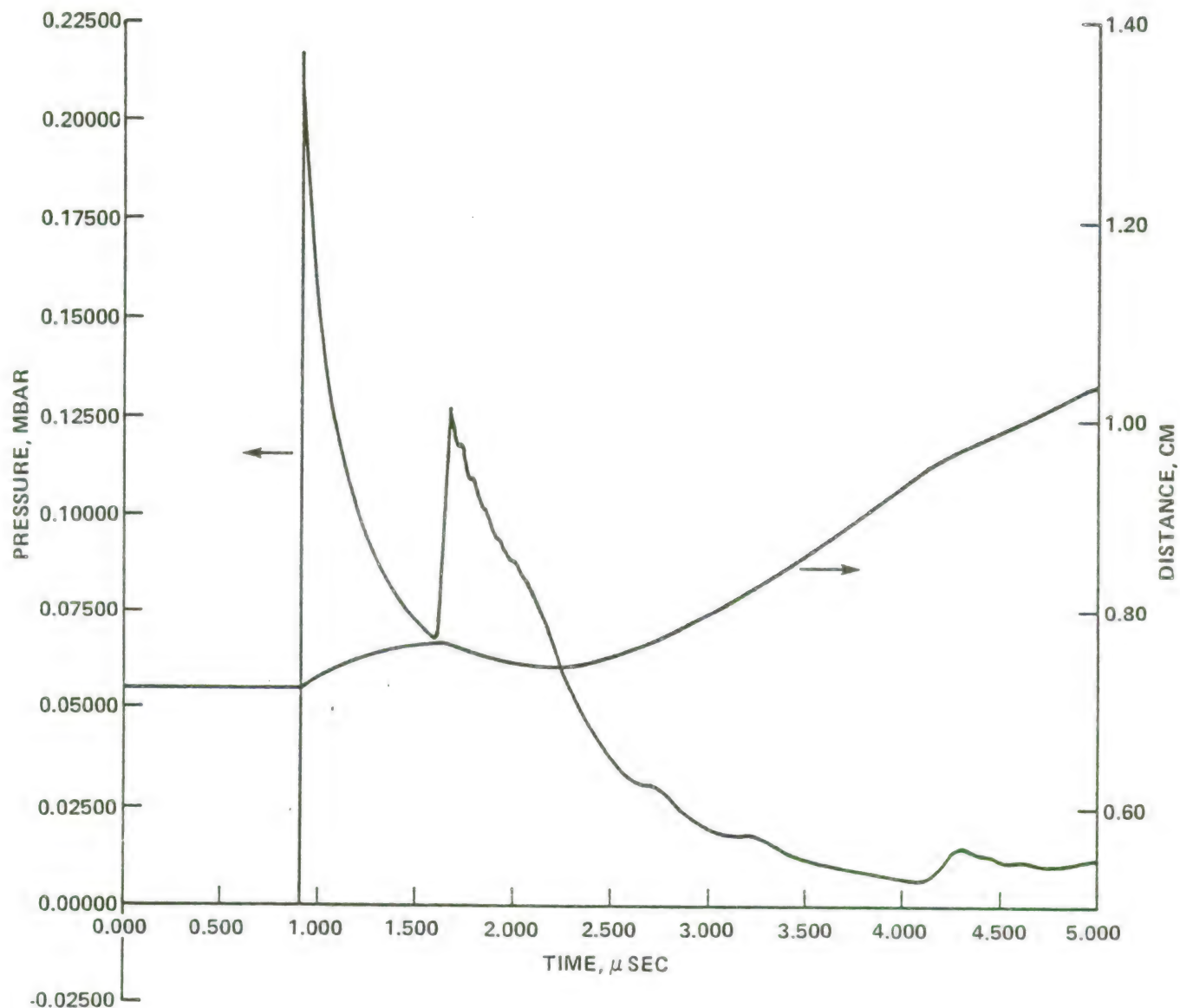


FIGURE A-4. PRESSURE AND DISTANCE VS TIME FOR PARTICLE PATH L2

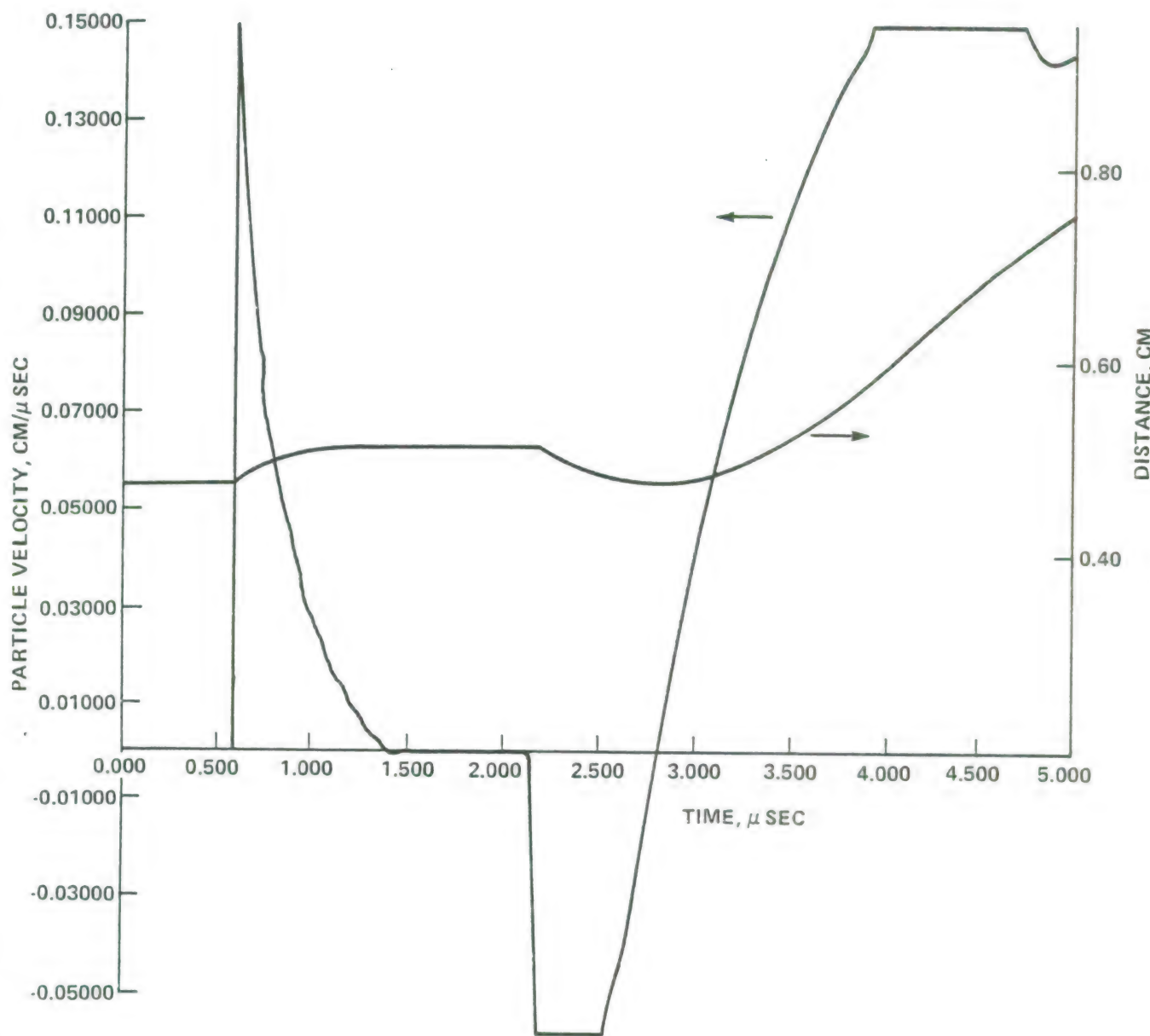


FIGURE A-5. PARTICLE VELOCITY AND DISTANCE VS TIME FOR PARTICLE PATH L1

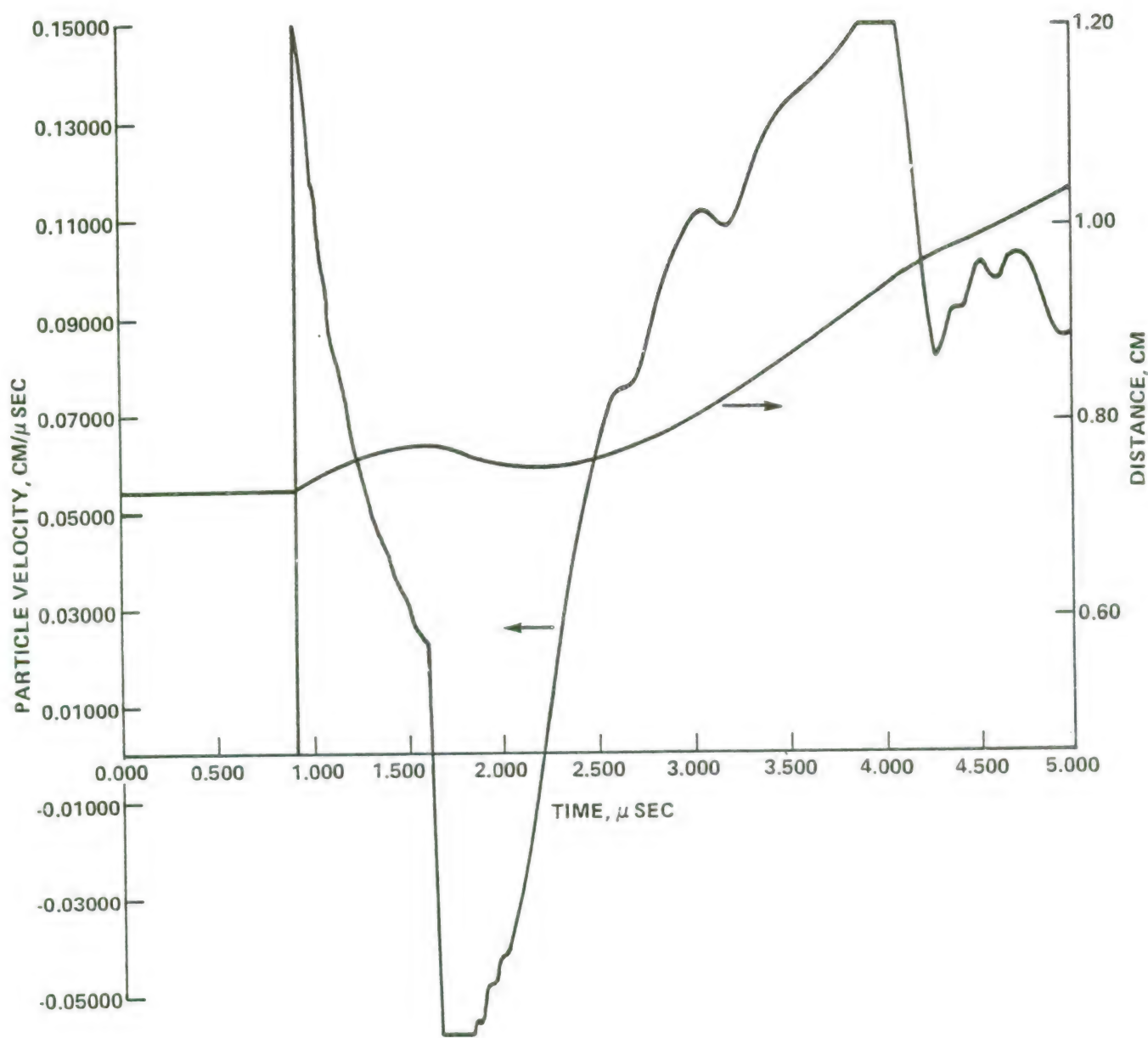


FIGURE A-6. PARTICLE VELOCITY AND DISTANCE VS TIME FOR PARTICLE PATH L2

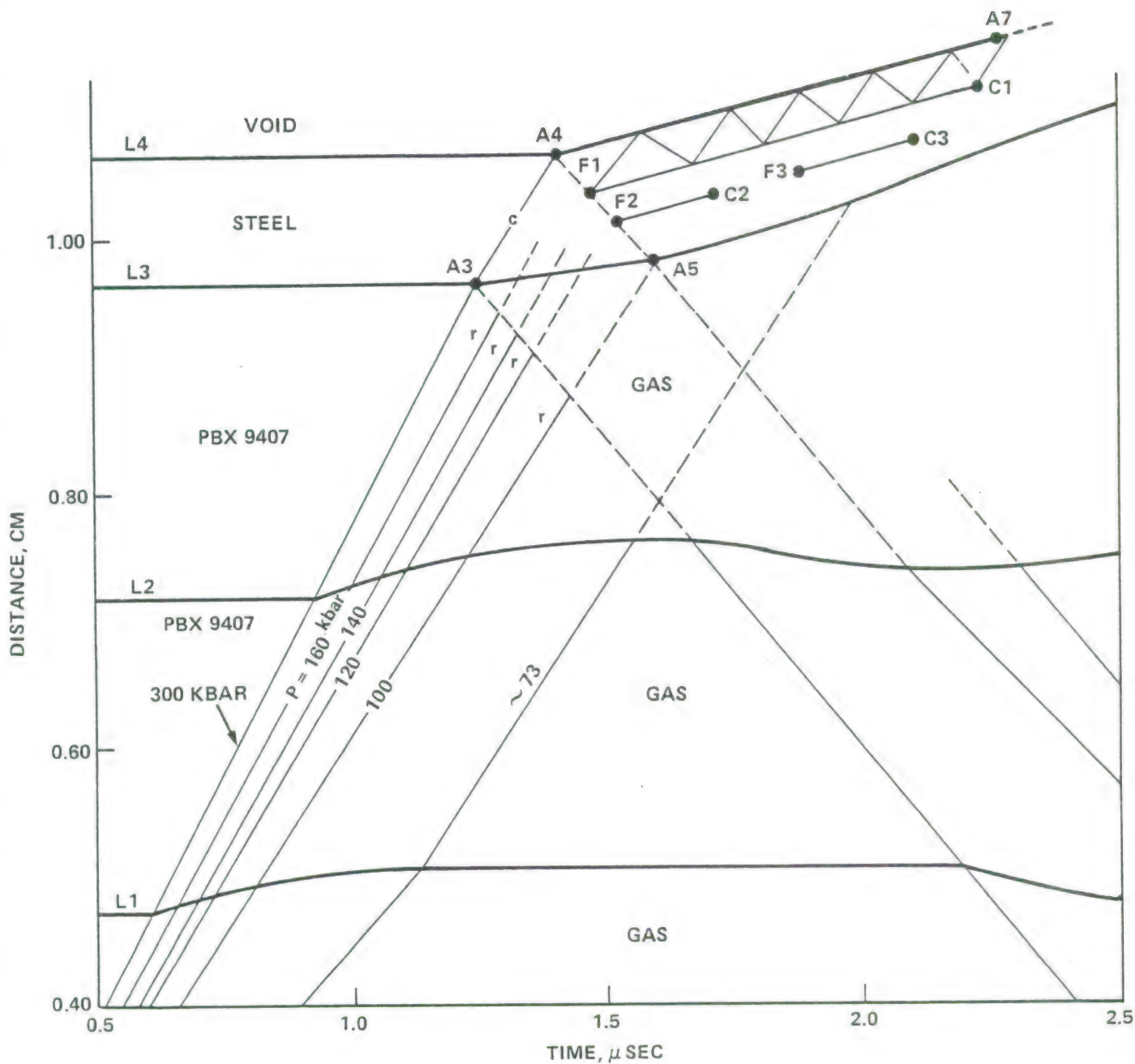


FIGURE A-7. DISTANCE VS TIME FOR WAVE INTERACTIONS IN THE COMPUTER MODEL
SHOWING EFFECT OF SPALLING

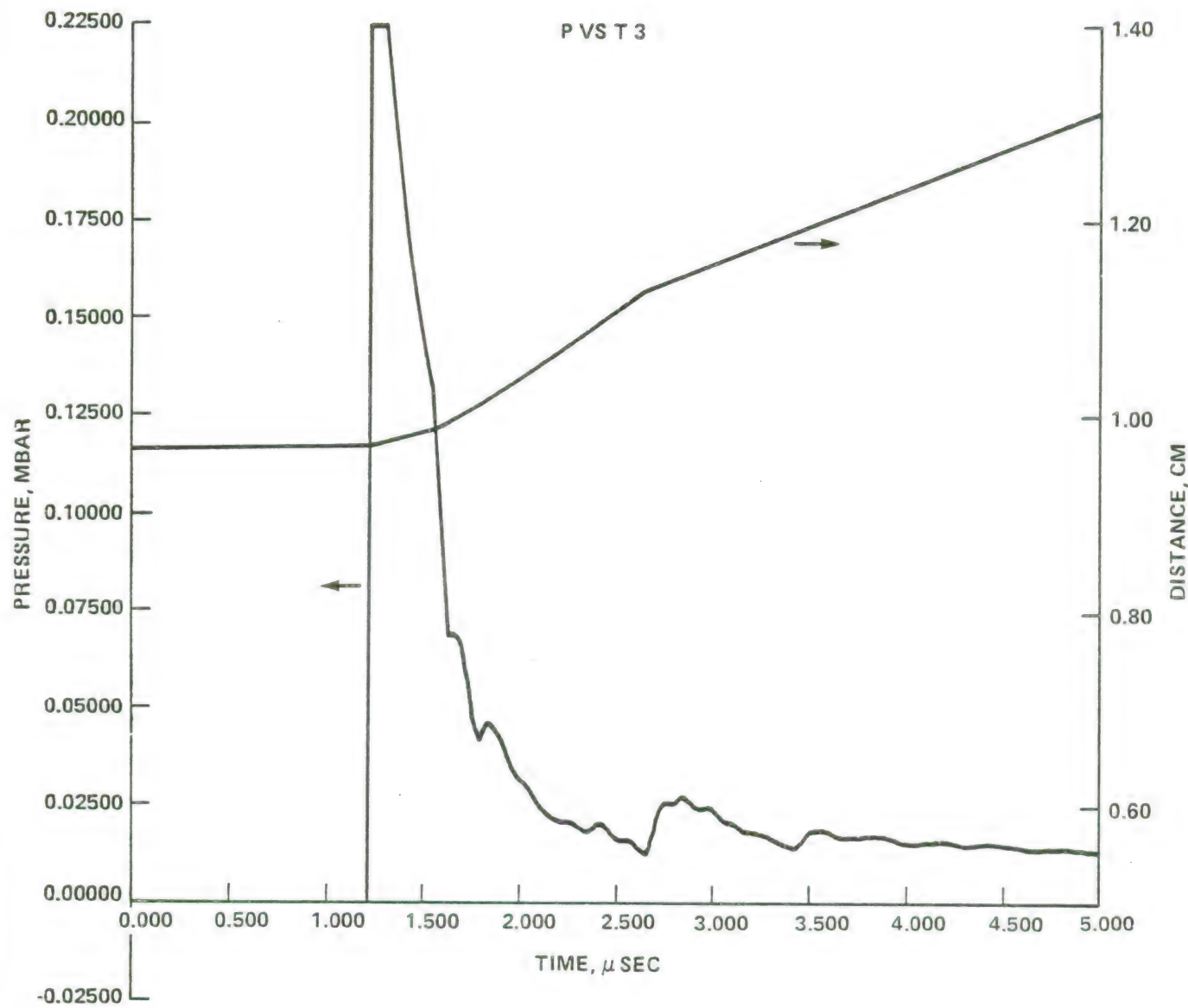


FIGURE A-8. PRESSURE AND DISTANCE VS TIME FOR PARTICLE PATH L3

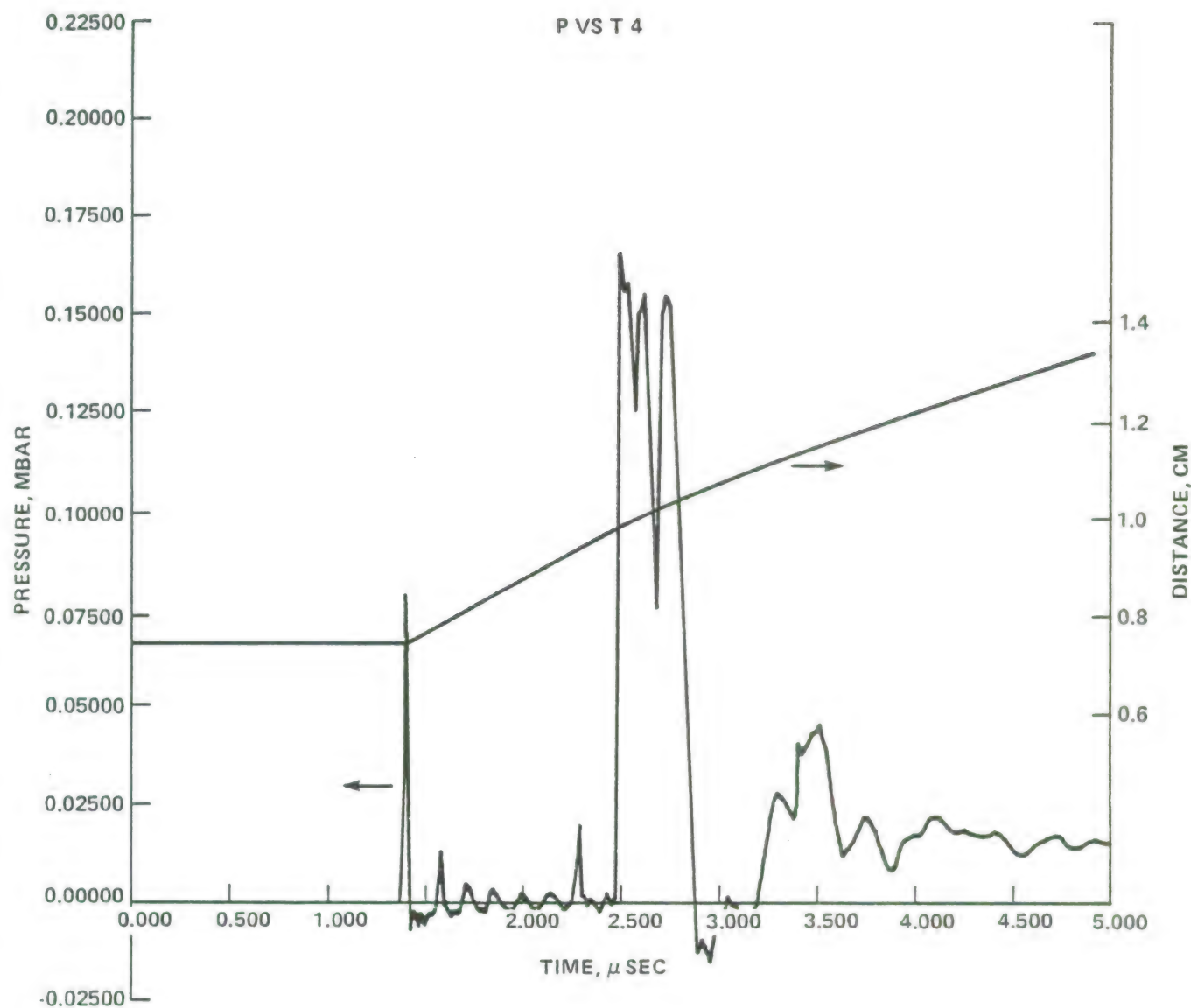


FIGURE A-9. PRESSURE AND DISTANCE VS TIME FOR PARTICLE PATH L4

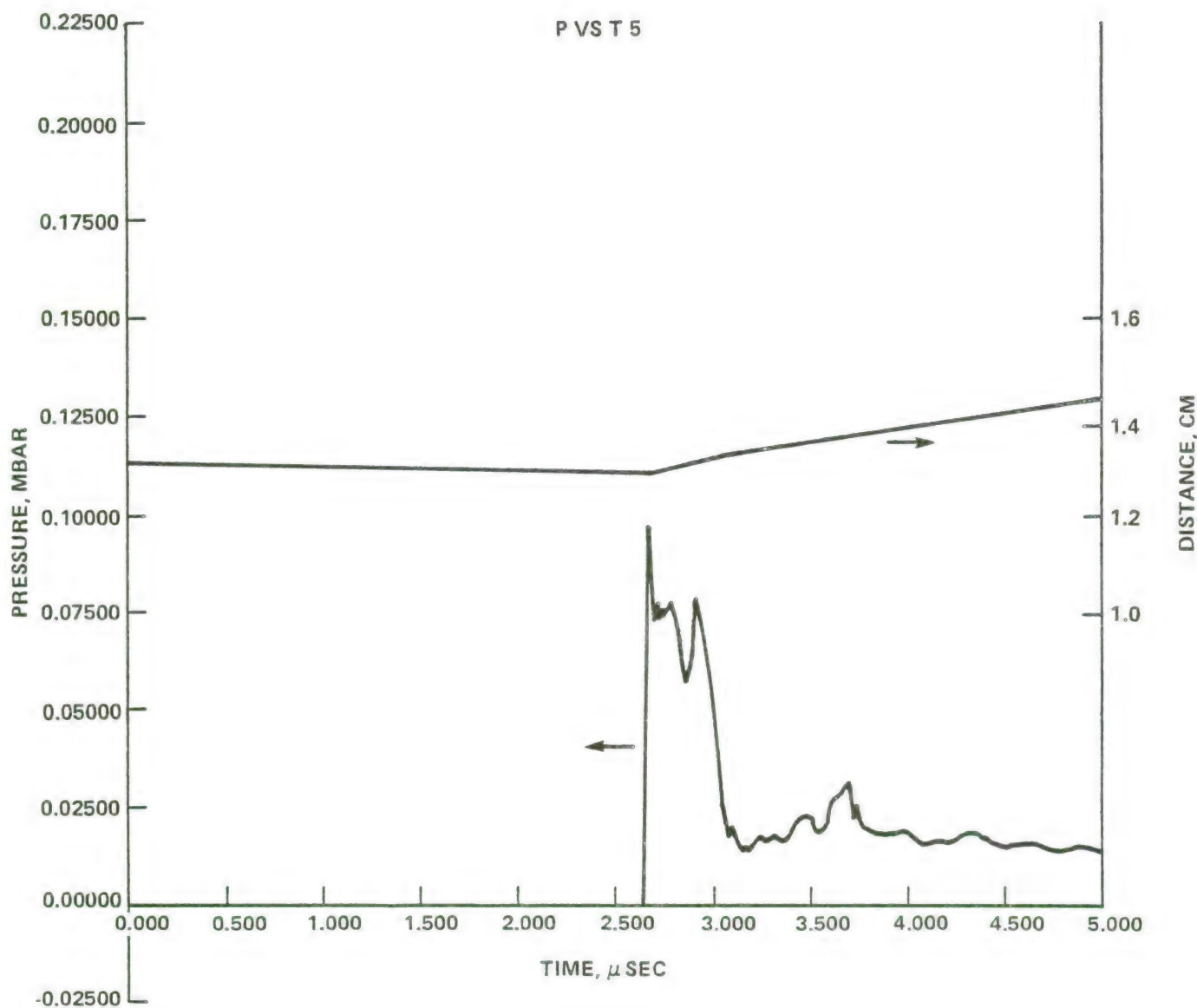


FIGURE A-10. PRESSURE AND DISTANCE VS TIME FOR PARTICLE PATH L5

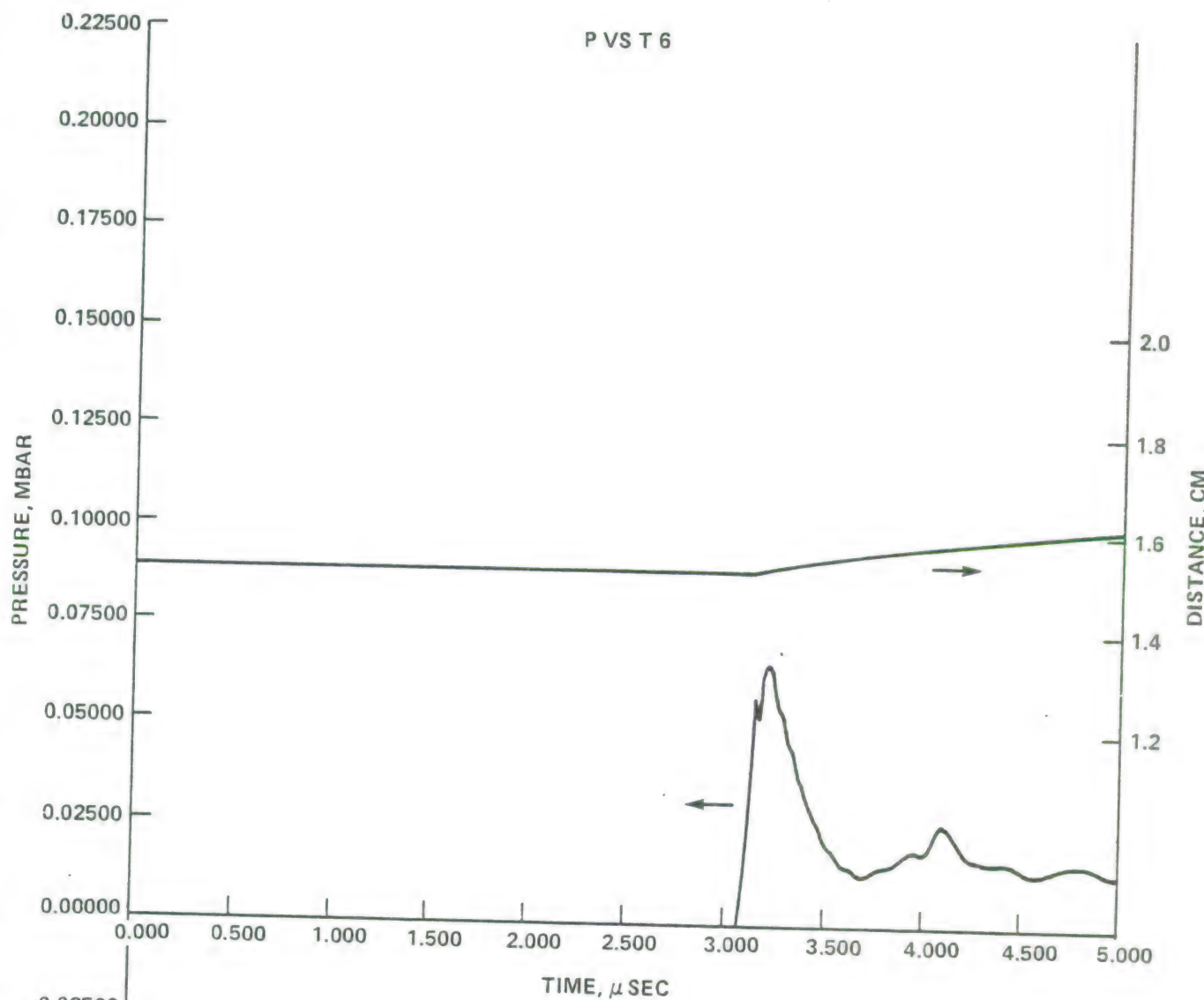


FIGURE A-11. PRESSURE AND DISTANCE VS TIME FOR PARTICLE PATH L6

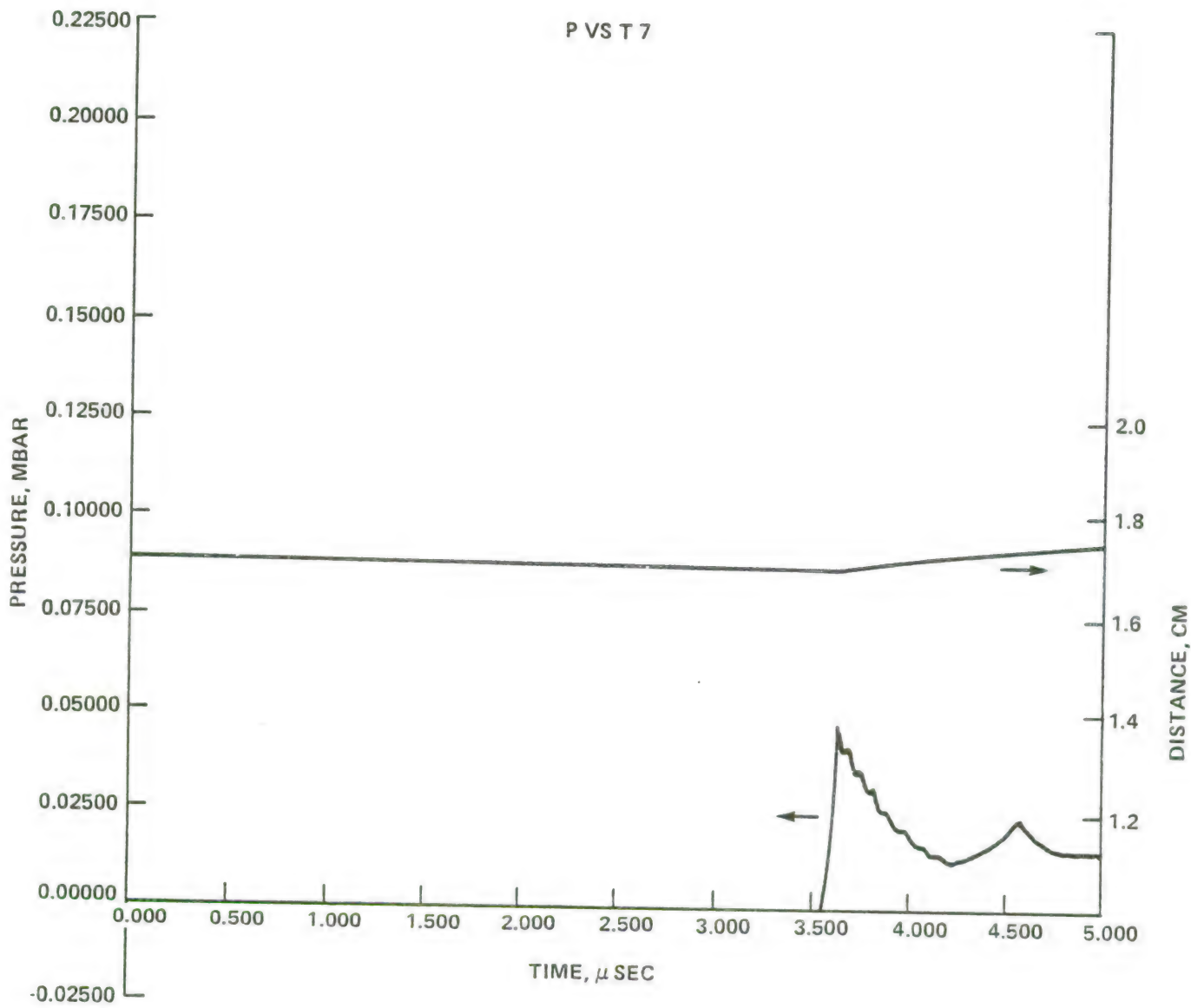


FIGURE A-12. PRESSURE AND DISTANCE VS TIME FOR PARTICLE PATH L7

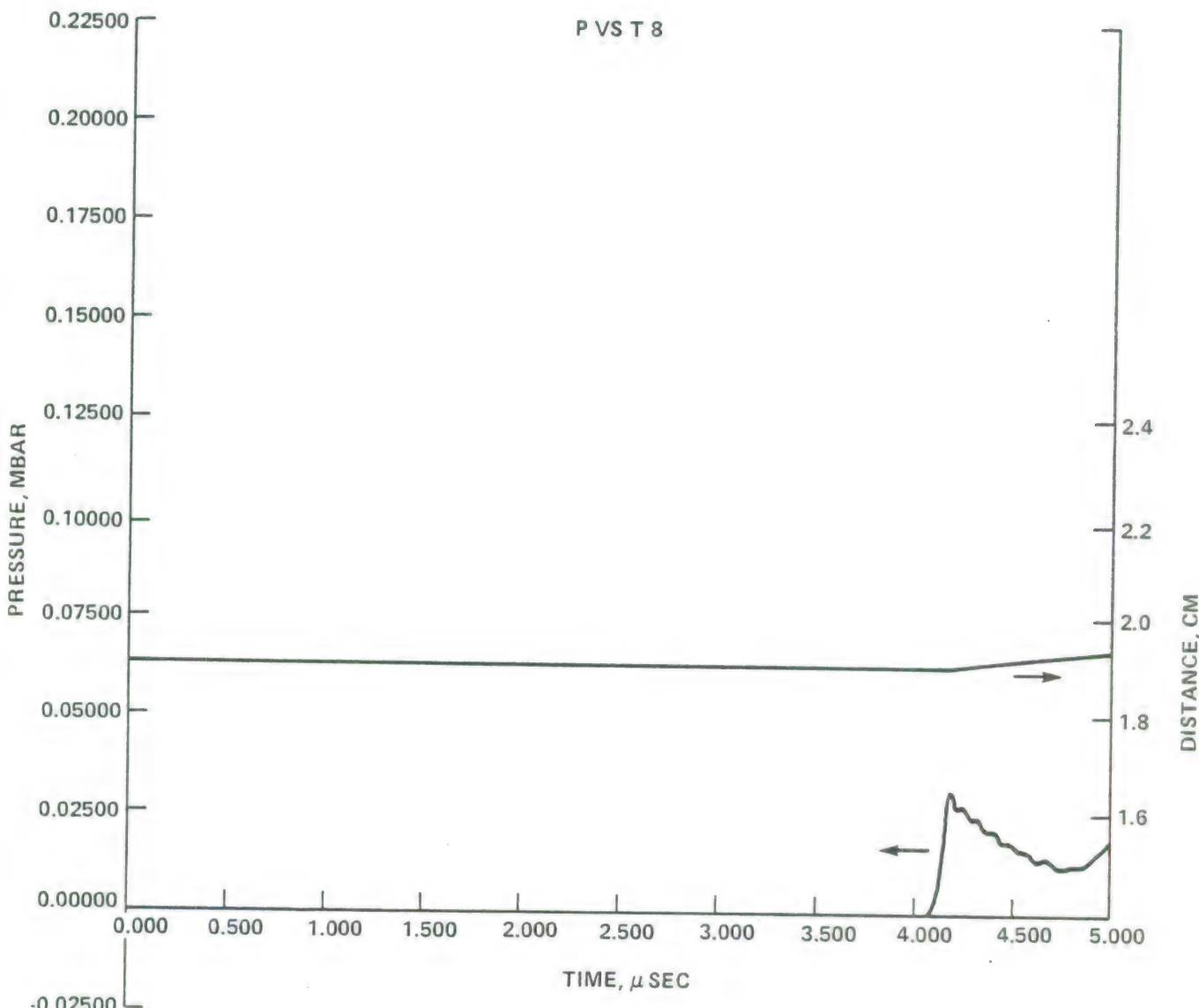


FIGURE A-13. PRESSURE AND DISTANCE VS TIME FOR PARTICLE PATH L8

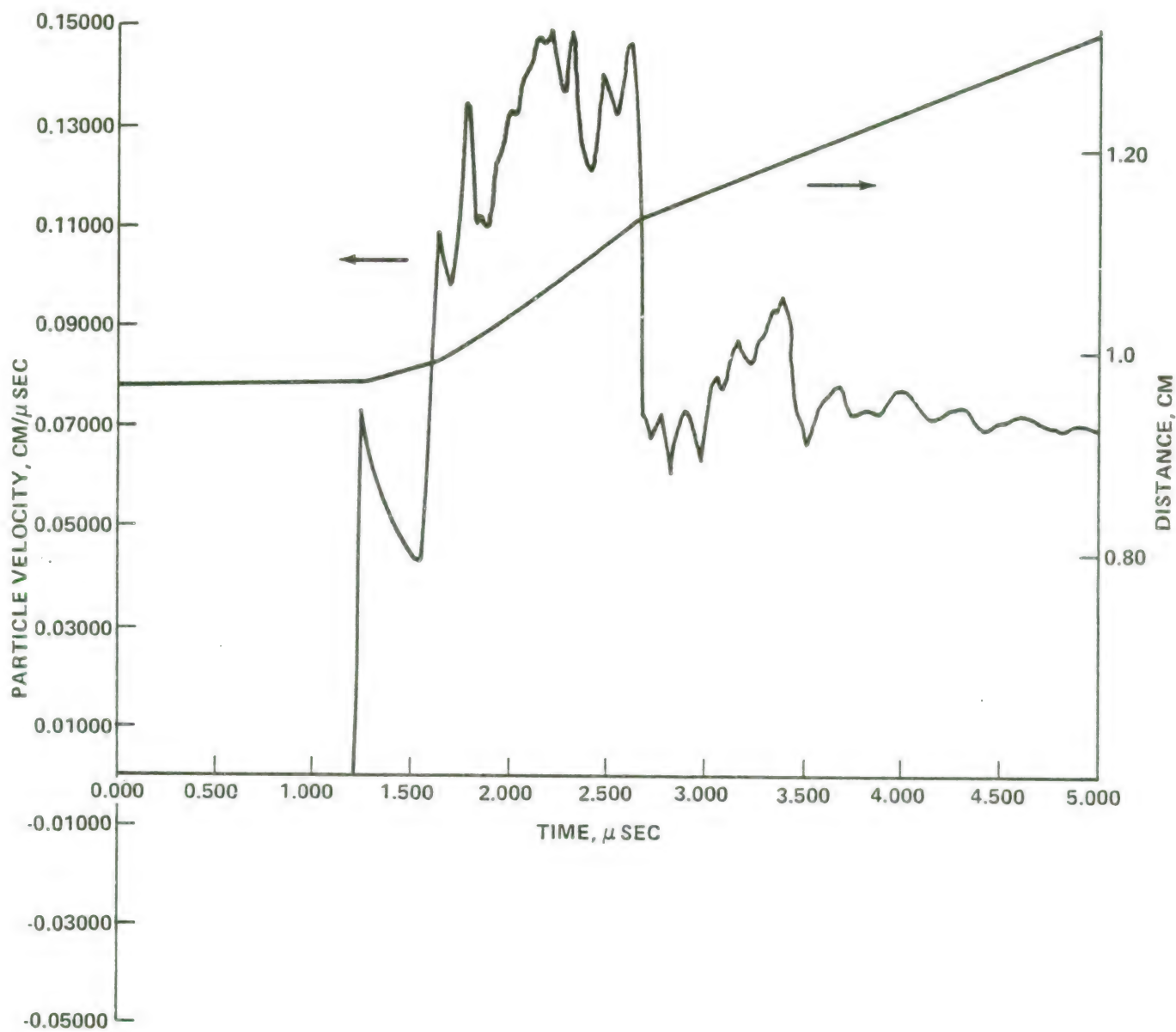


FIGURE A-14. PARTICLE VELOCITY AND DISTANCE VS TIME FOR PARTICLE PATH L3

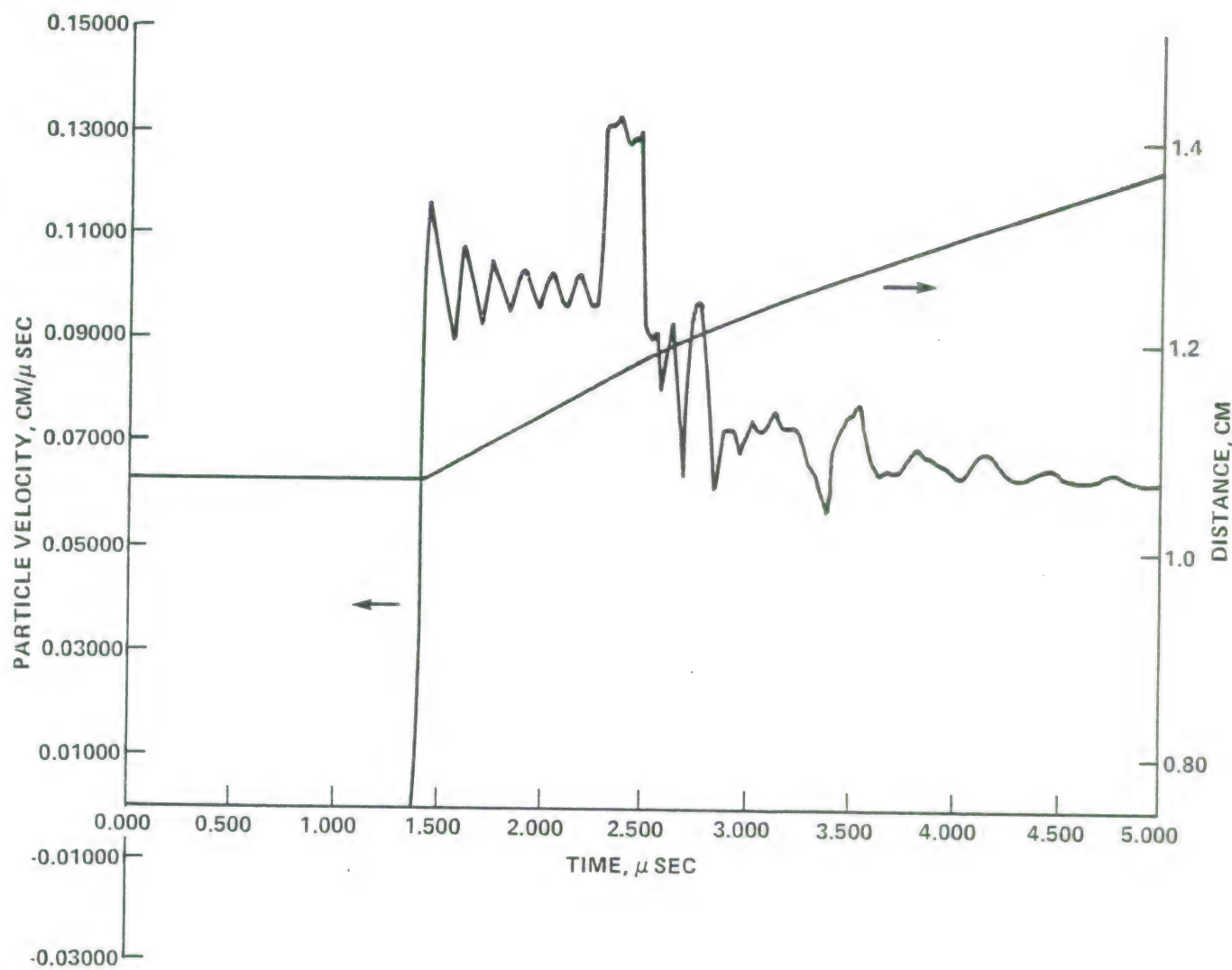


FIGURE A-15. PARTICLE VELOCITY AND DISTANCE VS TIME FOR PARTICLE PATH L4

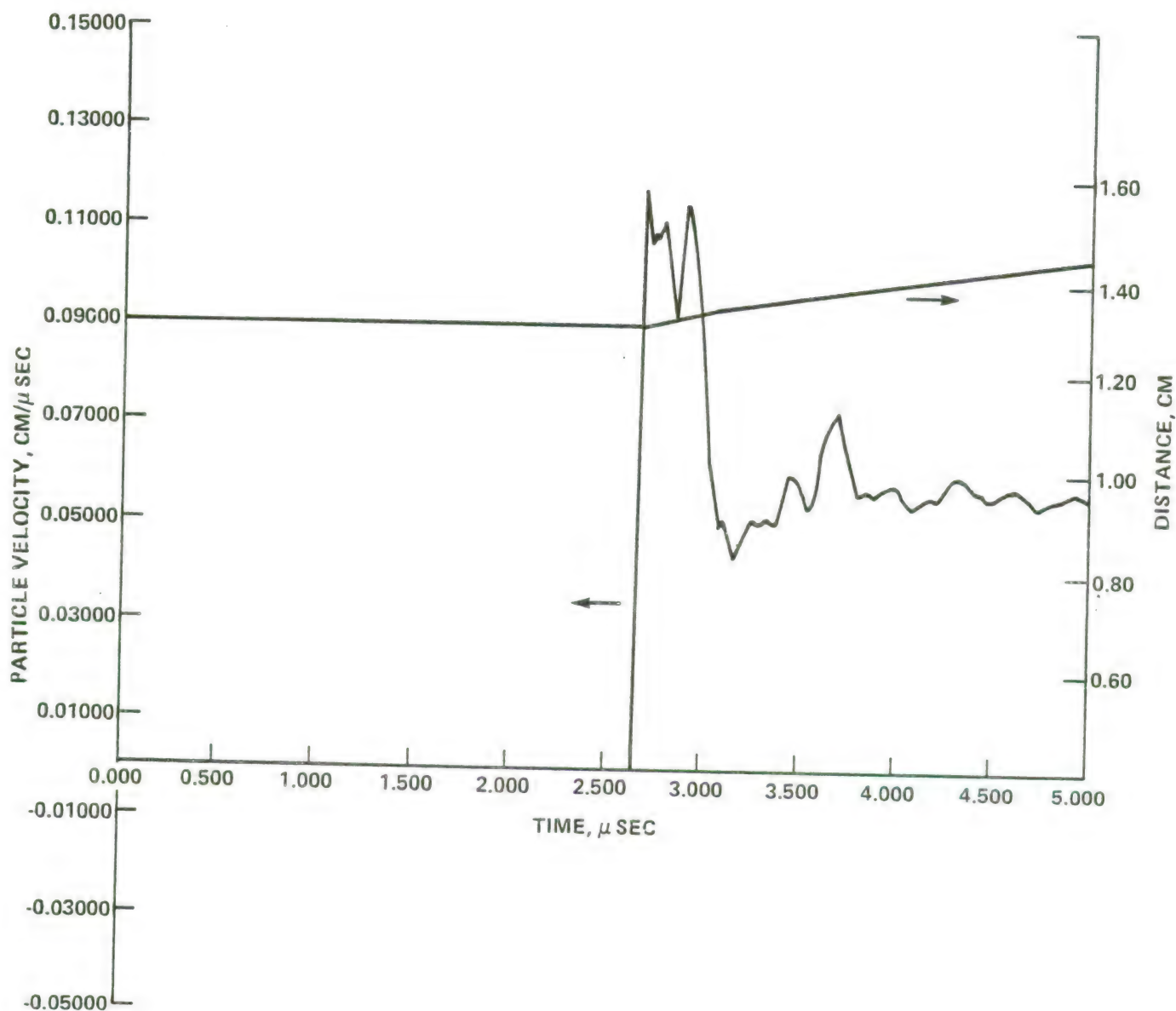


FIGURE A-16. PARTICLE VELOCITY AND DISTANCE VS TIME FOR PARTICLE PATH L5

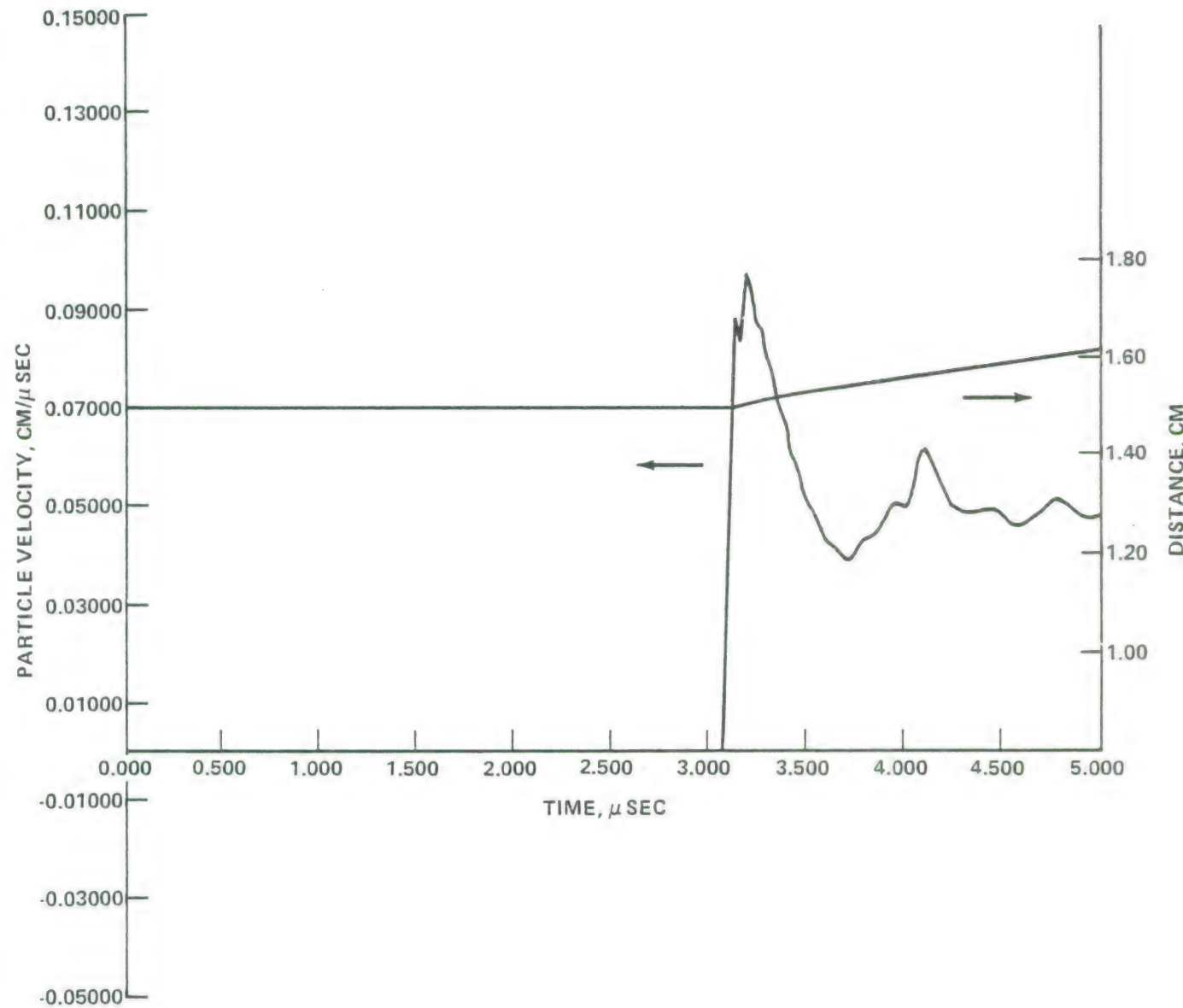


FIGURE A-17. PARTICLE VELOCITY AND DISTANCE VS TIME FOR PARTICLE PATH L6

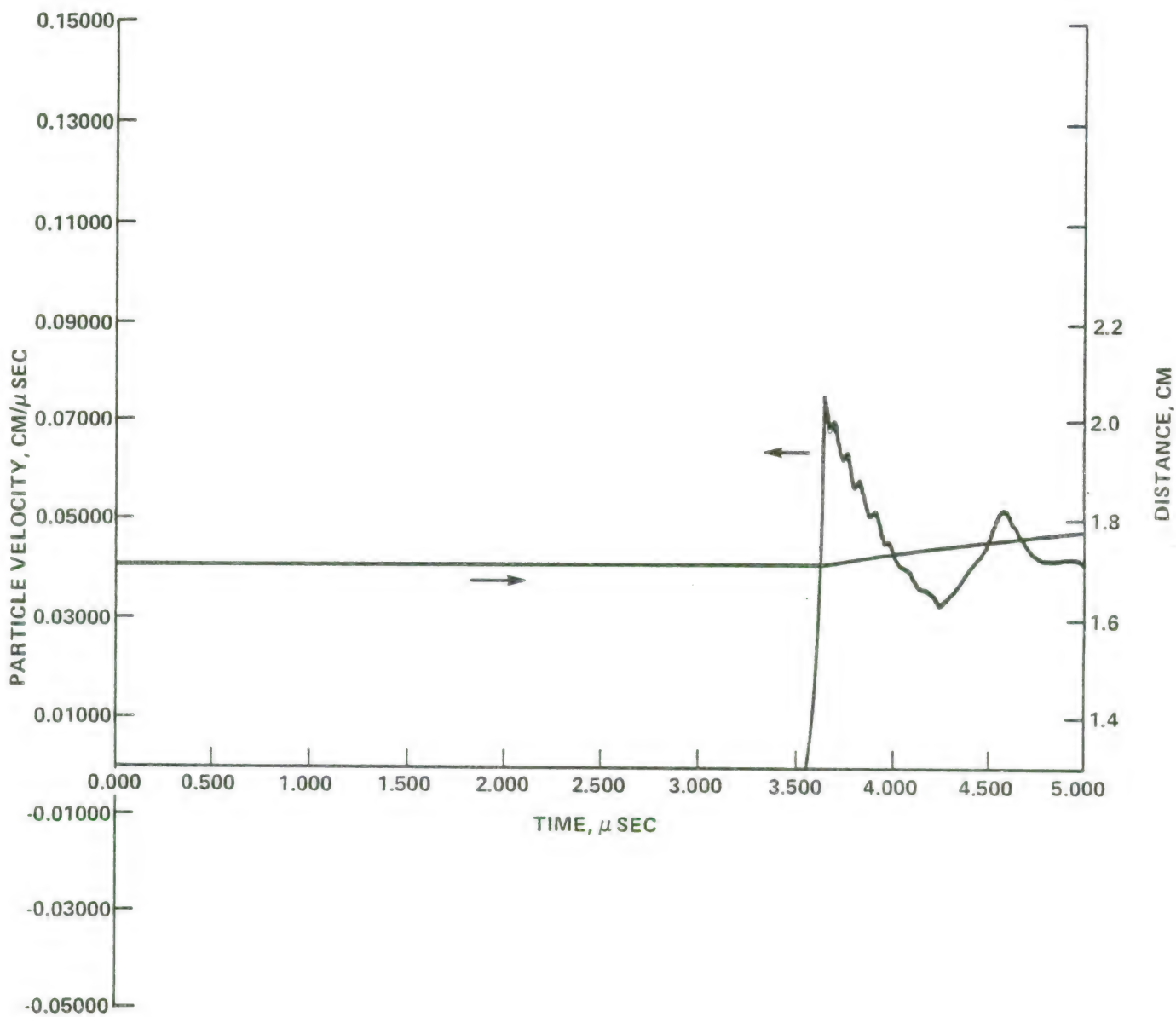


FIGURE A-18. PARTICLE VELOCITY AND DISTANCE VS TIME FOR PARTICLE PATH L7

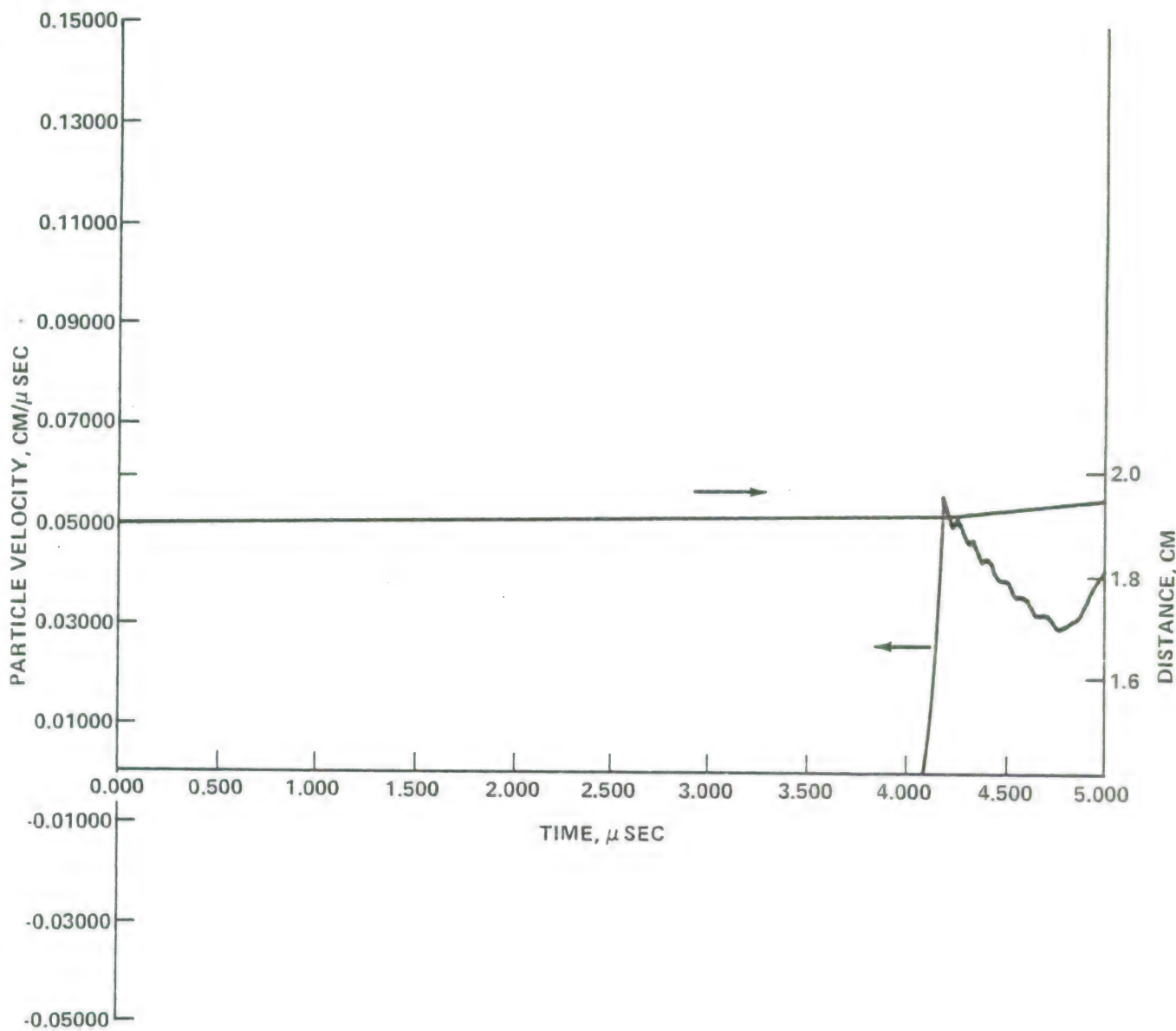


FIGURE A-19. PARTICLE VELOCITY AND DISTANCE VS TIME FOR PARTICLE PATH L8

REFERENCES

- A-1. Lutzky, M., Numerical Procedures For Testing Varidrive Assumptions, NSWC TR 82-542, 1 Aug 1982.
- A-2. Lawrence, R. J., and Mason D. S., Wondy IV - A Computer Program for One-Dimensional Wave Propagation with Rezoning, SC-RR-284, Sandia Laboratories, Aug 1971.
- A-3. Shapiro, Ascher H., The Dynamics and Thermodynamics of Compressible Fluid Flow, (New York: The Ronald Press Company), 1953.
- A-4. Fowles, G. R., "Experimental Technique and Instrumentation," Dynamic Response of Materials to Intense Impulsive Loading, Edited by Pei Chi Chow and Alan K. Hopkins, Air Force Materials Laboratory.
- A-5. Davison, L., and Graham, R. A., "Shock Compression of Solids," Physics letters, Vol. 55, No. 4, Oct 1979.
- A-6. Erkman, J. O., et. al., Calibration of the NOL Large Scale Gap Test; Hugoniot Data for Polymethyl Methacrylate, NOLTR 73-15, Apr 1973.

DISTRIBUTION

<u>Copies</u>	<u>Copies</u>
Chief of Naval Research 800 N. Quincy St. Arlington, VA 22217	
Commanding Officer Naval Explosive Ordnance Disposal Facility Attn: Library Division Indian Head, MD 20640	
Superintendent Attn: Library (Code 2124) Naval Postgraduate School Monterey, CA 93940	
Commander Naval Weapons Center Attn: Technical Library D. Lind P. Yates G. Greene R. G. Sewell China Lake, CA 93555	
Commanding Officer Naval Ship Research and Development Center Underwater Explosions Research Division Attn: Technical Reference Center Portsmouth, VA 23709	
Commanding Officer Naval Coastal Systems Center Attn: Technical Library Panama City, FL 32401	
Commander Naval Air Systems Command Attn: AIR-54111A AIR-541 AIR-4104 AIR-350 Washington, DC 20361	1 1 1 1 1
Commander Naval Ocean Systems Center Attn: Technical Library San Diego, CA 92152	1
Chief of Naval Operations Attn: OP-374 Technical Library Department of the Navy Washington, DC 20350	1
Commanding Officer Naval Ordnance Station Attn: Technical Library Indian Head, MD 20640	1
Commanding Officer Naval Weapons Station Attn: J. Carlson Y. McGann Library Yorktown, VA 23691	1 1 1

DISTRIBUTION (Cont.)

<u>Copies</u>		<u>Copies</u>	
Director Naval Research Laboratory Attn: Technical Information Washington, DC 20390		Chief of Research and Development 1 Department of the Army Washington, DC 20315	1
Commanding Officer Naval Torpedo Station Keyport, WA 98345		Army Material Command Attn: R & D Division 1 Department of the Army Washington, DC 20360	1
Strategic Systems Project Office Department of the Navy Attn: Technical Library Washington, DC 20376		Commanding General U.S. Army Weapons Command 1 Attn: G. Taylor Rock Island, IL 61201	1
Commander Pacific Missile Test Center Attn: Code 2141 Code 2200 Point Mugu, CA 93041		Commanding Officer Air Force Armament Laboratory 1 Attn: Library M. Zimmer Eglin, FL 35342	1 1 1
Director Development Center Marine Corps Development and Educational Command Quantico, VA 22134		Air Force Systems Command Andrews Air Force Base Attn: Phil Boesch, Chairman, 1 JTCG/MD Washington, DC 20331	1
Director Army Ballistic Research Laboratories Attn: Technical Library P. M. Howe DRDAR-BLT (D. Silva) Aberdeen Proving Ground Aberdeen, MD 21005		Commander Air Force Weapons Laboratory 1 Attn: SUL (Technical Library) Kirtland AFB, NM 87117	1
Commanding Officer ARRADCOM Attn: F. Finn Library SMUPA-DF (F. Saxe) LC (C. Cavanaugh) ASF (H. McGrady) LCU-CP (M. Margolin) LCE-E (R. Colucci) Dover, NJ 07801		Wright-Patterson AFB Attn: Systems Engineering Group (RTD) 1 Dayton, OH 45433	1
		Commander U.S. Army TECOM 1 Attn: L. Neally Aberdeen Proving Ground, MD 21005	1

DISTRIBUTION (Cont.)

DISTRIBUTION (Cont.)

Copies

Internal Distribution:

E231	2
E232	15
R10C (L. Roslund)	1
R10F (R. Bernecker)	1
R12 (J. Short)	1
R12 (J. Erkman)	5
R12 (M. Lutzky)	5
R12 (D. Chung)	1
R12 (L. Montesi)	1
R12 (P. Spahn)	1
R12 (T. Spivac)	1
R12 (P. Walter)	1
R13 (C. Dickinson)	1
R13 (J. Forbes)	1
R13 (K. Kim)	1
R13 (E. Lemar)	1
R13 (H. Sandusky)	1
R13 (G. Sutherland)	1
R13 (F. Zerilli)	1

BLANK

